ARTICLES
https://doi.org/10.1038/s41564-022-01153-5
nature microbiology

Check for updates

The DarTG toxin-antitoxin system provides phage defence by ADP-ribosylating viral DNA

Michele LeRoux[1], Sriram Srikant[1], Gabriella I. C. Teodoro[1], Tong Zhang[1], Megan L. Littlehale[1], Shany Doron[2], Mohsen Badiee[3], Anthony K. L. Leung[3,4], Rotem Sorek[2] and Michael T. Laub[1,5] ✉

Toxin-antitoxin (TA) systems are broadly distributed, yet poorly conserved, genetic elements whose biological functions are unclear and controversial. Some TA systems may provide bacteria with immunity to infection by their ubiquitous viral predators, bacteriophages. To identify such TA systems, we searched bioinformatically for those frequently encoded near known phage defence genes in bacterial genomes. This search identified homologues of DarTG, a recently discovered family of TA systems whose biological functions and natural activating conditions were unclear. Representatives from two different subfamilies, DarTG1 and DarTG2, strongly protected *E. coli* MG1655 against different phages. We demonstrate that for each system, infection with either RB69 or T5 phage, respectively, triggers release of the DarT toxin, a DNA ADP-ribosyltransferase, that then modifies viral DNA and prevents replication, thereby blocking the production of mature virions. Further, we isolated phages that have evolved to overcome DarTG defence either through mutations to their DNA polymerase or to an anti-DarT factor, gp61.2, encoded by many T-even phages. Collectively, our results indicate that phage defence may be a common function for TA systems and reveal the mechanism by which DarTG systems inhibit phage infection.

Bacteriophages, or phages, are the nearly ubiquitous viruses that infect bacteria. Their co-evolution with bacteria has led to an abundance of anti-phage defence systems. CRISPR and restriction-modification systems are two well-known systems that have been extensively characterized and famously co-opted as indispensable tools for molecular biology. In recent years, due to a recognition of the vast, unexplored biological potential of such systems, and the renewed interest in phage therapy as an alternative to antibiotics, there has been an explosion in the number of newly identified phage defence systems[1–4]. However, in most cases, the mechanism of action of these phage defence systems remain unknown or incompletely elucidated.

One class of genetic elements increasingly implicated in phage defence are toxin-antitoxin (TA) systems, which are found in nearly all sequenced bacterial chromosomes, with some species encoding dozens of different systems[5,6]. These systems typically feature a two-gene operon that encodes a growth-inhibiting toxin and a cognate neutralizing antitoxin, which is often less stable than the toxin[5]. TA systems are categorized on the basis of the nature of the antitoxin, with the four most common types featuring a small non-coding RNA that prevents toxin translation (type I), a protein that directly interacts with and neutralizes the toxin (type II), a non-coding RNA that directly interacts with the toxin (type III), or a protein that enzymatically reverses the activity of the toxin (type IV)[5].

The biological functions of chromosomally-encoded TA systems have remained elusive and controversial[5,7–9]. Cells expend substantial resources in keeping these systems in an 'off' state, in which toxin is neutralized by antitoxin[10]. Despite the seemingly high cost of their maintenance, the prevalence of TA systems suggests that they are important for bacterial survival. TA systems are often postulated to be stress-response elements[8,11], but we previously found in *Escherichia coli* MG1655 that although stress can drive transcriptional induction of its 10 endoribonuclease toxins, active toxins do not get released[10]. Increasing evidence suggests that some TA systems function in phage defence, which may explain both their variability and ubiquity[6]. One of the best characterized examples are type III ToxIN systems, first identified in *Pectobacterium atrosepticum*, which feature an endoribonuclease toxin, ToxN[12]. For a ToxIN system found in some *E. coli* strains, it was recently shown that toxin is liberated following phage-induced shutoff of host transcription and subsequent degradation of the unstable antitoxin[13]. The toxin then cleaves phage mRNAs to prevent translation of key structural components. Another well-characterized phage defence TA system is RnlAB, a type II system whose toxin is also an RNase[14]. For most other TA systems that function in phage defence, the toxin's mechanism of action has only been studied by overexpression, not during infection, so how they disrupt the phage life cycle is unclear. However, given the remarkable diversity of biochemical functions ascribed to toxins beyond RNases, TA systems may block phage development at different stages in many different ways.

We set out to identify additional TA systems that provide phage defence by identifying systems frequently found near other phage defence elements. Phage defence systems are often co-located on bacterial chromosomes in so-called defence islands[15,16]. Efforts to identify genes of unknown function that are frequently found in such genomic contexts have proven to be a fruitful strategy for identifying new phage defence systems[3,4]. Applying this same approach specifically to TA systems led to the identification of two systems, DarTG1 and DarTG2, that can provide *E. coli* with potent defence against select phage. Previous work on DarTG systems demonstrated that DarT toxins can use NAD+ to ADP-ribosylate DNA, and artificial overexpression of these toxins can disrupt chromosomal DNA replication[17–20]. However, our work now demonstrates that under the

[1]Department of Biology, Massachusetts Institute of Technology, Cambridge, MA, USA. [2]Department of Molecular Genetics, Weizmann Institute of Science, Rehovot, Israel. [3]Department of Biochemistry and Molecular Biology, Bloomberg School of Public Health, Johns Hopkins University, Baltimore, MD, USA. [4]Department of Molecular Biology and Genetics, Department of Genetic Medicine, Department of Oncology, School of Medicine, Johns Hopkins University, Baltimore, MD, USA. [5]Howard Hughes Medical Institute, Massachusetts Institute of Technology, Cambridge, MA, USA. ✉e-mail: laub@mit.edu

natural activating conditions of phage infection, the DarT toxins in fact ADP-ribosylate phage DNA, which inhibits both viral DNA and RNA synthesis. Without new copies of their genomes to package, phages are unable to form progeny. Phages can evolve to overcome DarT activity by two different strategies, either mutating their DNA polymerase, probably to bypass ADP-ribosylation in the DNA, or by modifying an existing anti-DarT factor. In sum, our work demonstrates that DarTG systems can provide cells with strong defence against phage infection through the ADP-ribosylation of phage DNA. More generally, our work underscores the notion that the enzymatically diverse toxins of TA systems may equip bacteria with a diverse arsenal of phage defence mechanisms.

Results

DarTG systems provide defence against phage. We set out to examine the propensity of ten common type II TA systems to be present in defence islands, a property previously found as predictive for function in phage resistance[3]. To this end, we analysed the genomic context of 202,402 toxin genes found in ~38,000 bacterial and archaeal genomes. For each type of toxin, we calculated a 'defence score' as the fraction of toxin homologues found within ten genes of known phage defence genes (Supplementary Table 1). It was previously shown that defence scores >0.4 are strongly predictive of anti-phage activity[3]. In our analysis, one TA family, the DarTG system, stood out with a defence score of 0.48, meaning that nearly half of the genes encoding DarTG homologues in this family are next to known defence genes in microbial genomes. Previous work had noted that *darTG* is sometimes found encoded within type I restriction-modification system operons[17].

DarTG systems have not been previously shown to function in phage defence. To test whether they can indeed provide defence against phages, we cloned two DarTG systems. In each case, we included the open reading frames encoding the toxin and antitoxin, as well as the native upstream region encompassing the promoter. These systems were cloned into a pBR322 vector backbone and transformed into *E. coli* MG1655. Each system was then tested against a panel of 12 phages that can infect MG1655 in both fast and slow growth conditions (LB medium at 37 °C, fast growth; M9-glucose medium at 30 °C, slow growth) (Fig. 1a–c). Both systems provided robust defence against different phages under different conditions. DarTG1 prevented plaquing of RB69 and T5 in fast growth conditions, while DarTG2 provided robust phage defence against T5, SECϕ18, and Lust in slow growth conditions, with modest protection against T5 in fast growth conditions. We also tested whether a single chromosomal copy of DarTG1 was sufficient to confer phage defence, and found that it did defend against RB69, albeit with less potency (Fig. 1d).

The genes encoding the DarTG1 and DarTG2 systems that we cloned were not near other known defence systems but were each within prophages in *E. coli* strains C7 and 2-460-02_S4_C3, respectively (Fig. 1e). Homologues of the DarT toxins were previously shown to be single-stranded DNA ADP-ribosyltransferases[17,19]. A multiple sequence alignment of DarT homologues (often annotated as containing DUF4433), including the ones we cloned and those previously characterized biochemically, revealed high similarity across the entire length of the proteins (Fig. 1f(top) and Extended Data Fig. 1). There was complete conservation of many residues including a glutamate (E152 and E147 in the cloned DarT1 and DarT2, respectively) (Fig. 1f, red highlight) known to be critical for catalysis of these ssDNA ADP-ribosyltransferases[17,19]. We mutated this conserved glutamate to an alanine in both DarT1 and DarT2 and found that phage defence was abolished in each case (Fig. 1b,c). Hereafter, we refer to these inactive mutant versions of the TA systems as DarT*G1 and DarT*G2.

In contrast to the DarT toxins, a multiple sequence alignment of their cognate DarG antitoxins revealed two distinct families (Fig. 1f(bottom) and Extended Data Fig. 2). DarG1 contains a putative YbiA-like fold (80% confidence, Phyre2 prediction), a domain predicted to function in ADP-ribose processing[21], while DarG2 features a highly conserved, N-terminal macrodomain known to hydrolyse the ADP-ribose modifications introduced by their cognate toxins[17,22,23]. The C-terminal region of both proteins, which has been implicated in binding directly to DarT2[18], is conserved in both protein families.

DarTG-mediated phage defence functions by abortive infection. Phage defence often occurs via an abortive infection (Abi) mechanism in which the infected cell dies but no phage progeny is produced, thereby preventing spread of the virus in a population. Abi mechanisms are traditionally thought to result from a defence mechanism that directly kills the host cell, but can also arise if the defence mechanism targets the virus, with the host cell dying because the virus triggers irreversible damage, such as chromosome degradation. One key characteristic of Abi mechanisms is that when most cells are infected at a high multiplicity of infection (MOI), the growth of the bacterial population stops, while at lower MOIs, the uninfected bacteria can continue to grow. To test whether the DarTG systems trigger Abi, we infected cells harbouring either the native DarTG1 or the inactive DarT*G1 system with RB69 phage at varying MOIs, and tracked bacterial growth by measuring the optical density at 600 nm (OD_{600}) over time in microtitre plates (Fig. 2a and Extended Data Fig. 3a). At MOIs of 10 and 1, cells harbouring DarTG1 did not grow and the OD_{600} of the cultures decreased over time, indicating that cells were lysing. Consistent with this interpretation, we found that no viable cells remained 30 min post infection for either DarTG1- or DarT*G1-containing cells (Fig. 2c). At MOIs of 0.1 and 0.01, the OD_{600} of cultures harbouring DarTG1, but not DarT*G1, increased over time indicating that cell growth continued as DarTG1 prevents the phage infection from spreading throughout the population (Fig. 2a). Similar trends were seen for DarTG2 cells infected with T5 (Fig. 2b,d and Extended Data Fig. 3b). These data suggest that both DarTG1 and DarTG2 provide phage defence via an abortive infection mechanism.

We directly assessed the number of RB69 progeny produced in DarTG1- and DarT*G1-containing cells grown in shaking flasks during infection. For cells containing the inactive DarT*G1 system, the initial burst occurred about 25–30 min after infection and released ~100 phages (Fig. 2e). In contrast, when DarTG1 was present, no phage progeny were detected up to 45 min post infection. We obtained similar results for DarTG2 infected with T5 (Fig. 2f), although the burst size was smaller. Taken all together, our results support an abortive infection mechanism for DarTG-containing cells, in which activation of the toxin effectively thwarts the production of new phage particles, but infected cells do not survive.

We also tracked infected cells by time-lapse fluorescence microscopy, using the cell-permeable DNA dye 4',6-diamidino-2-phenylindole (DAPI) to stain both bacterial and phage DNA. Phage particles appear as extracellular puncta in the DAPI channel (Extended Data Fig. 4a) and thus phage infections can be visualized in real time, while DAPI staining of host DNA simultaneously allows tracking of bacterial cell lysis (Extended Data Fig. 4b). We found that cellular DNA appeared more compacted in the infected DarTG1-containing cells before lysis (Fig. 2g, 20 min timepoint and Extended Data Fig. 4c). In the infected DarT*G1-containing cells, the DNA appeared diffuse throughout the infection process, and following lysis, new phage particles appeared (Fig. 2g and Extended Data Fig. 4d). There are some DAPI-stained, extracellular puncta present around both DarTG1 and DarT*G1 cells before cell lysis, which are probably unadsorbed phage. The number of these extracellular puncta increased substantially following lysis of cells harbouring DarT*G1, but not DarTG1.

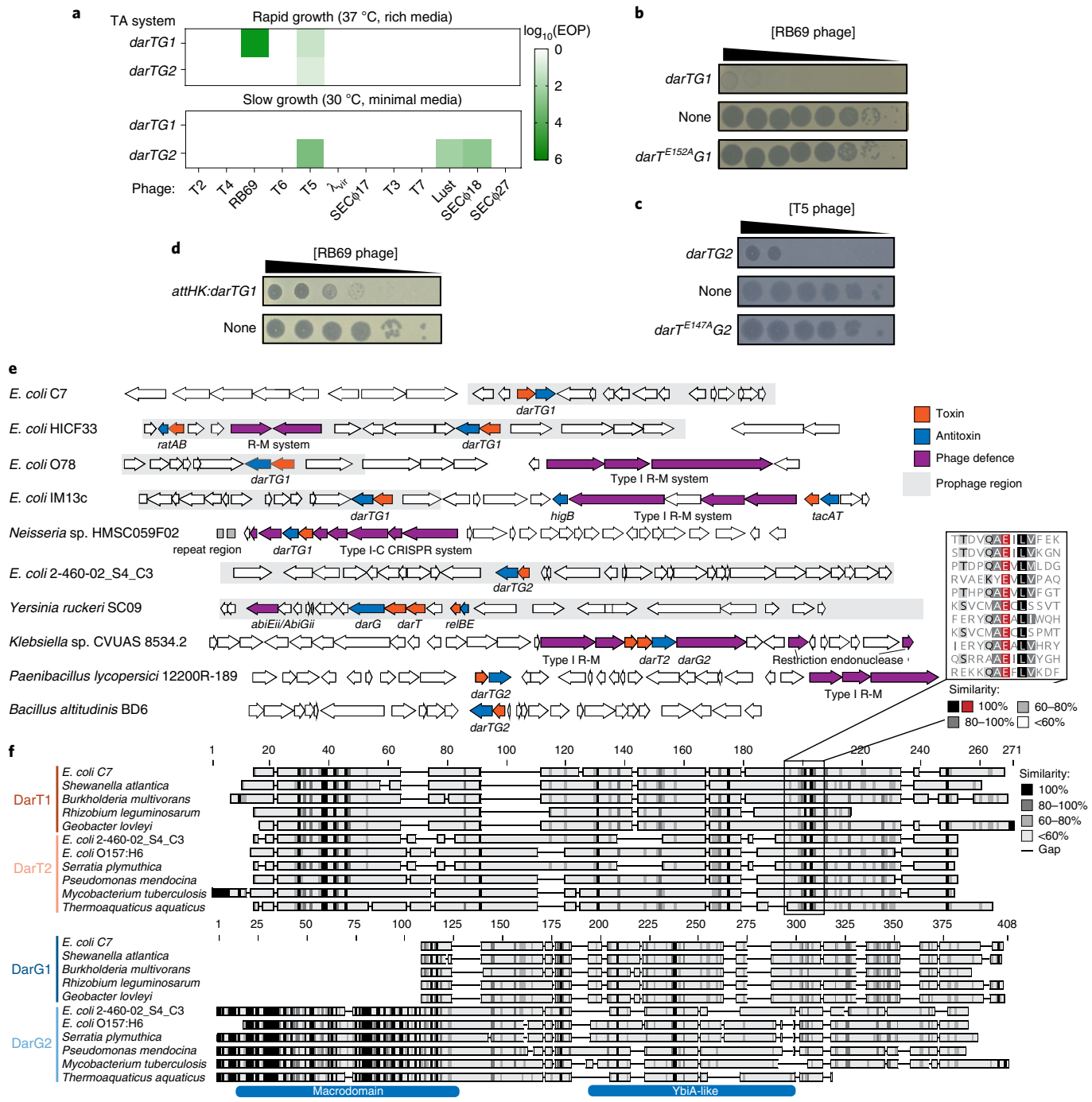

Fig. 1 | TA systems encoded near known phage defence elements also defend against phage. a, Efficiency of plaquing (EOP; indicated in green) for strains bearing the indicated DarTG systems infected with a panel of phages compared to a strain bearing an empty vector under two different growth conditions. **b**,**c**, Tenfold serial dilution plaque assays of RB69 (**b**) or T5 (**c**) phage spotted on *E. coli* MG1655 harbouring the indicated *darTG* system regulated by its native promoter (top), an empty vector (middle) or the *darTG*-bearing plasmid with a mutation in the predicted active site of the toxin (bottom). **d**, EOP for RB69 phage on *E. coli attHK::darTG1* compared to a wild-type MG1655 strain. **e**, Genomic context for the *darTG1* and *darTG2* systems in **b** and **c**, along with additional selected *darTG1*-like and *darTG2*-like systems, illustrating their frequent association with prophages and known phage defence elements. **f**, Multiple sequence alignments of representative DarT toxins and DarG antitoxins.

We found that T5 infections did not proceed effectively under time-lapse microscopy conditions, so we sampled from liquid cultures of DAPI-stained, T5-infected cells and imaged them at various time points after infection (Fig. 2h). Similar to DarTG1, we saw fewer DarTG2-containing cells lysing, combined with a dramatic difference in the appearance of new phage particles following infection of DarT*G2 versus DarTG2-containing cells. These microscopy experiments support an abortive infection mechanism for both DarTG systems and, at least for DarTG1, suggest that DarT may affect DNA.

Activated DarT inhibits DNA synthesis by ADP-ribosylating DNA. Previous studies demonstrated that ADP-ribosylation of chromosomal DNA by DarT, either following ectopic expression of DarT

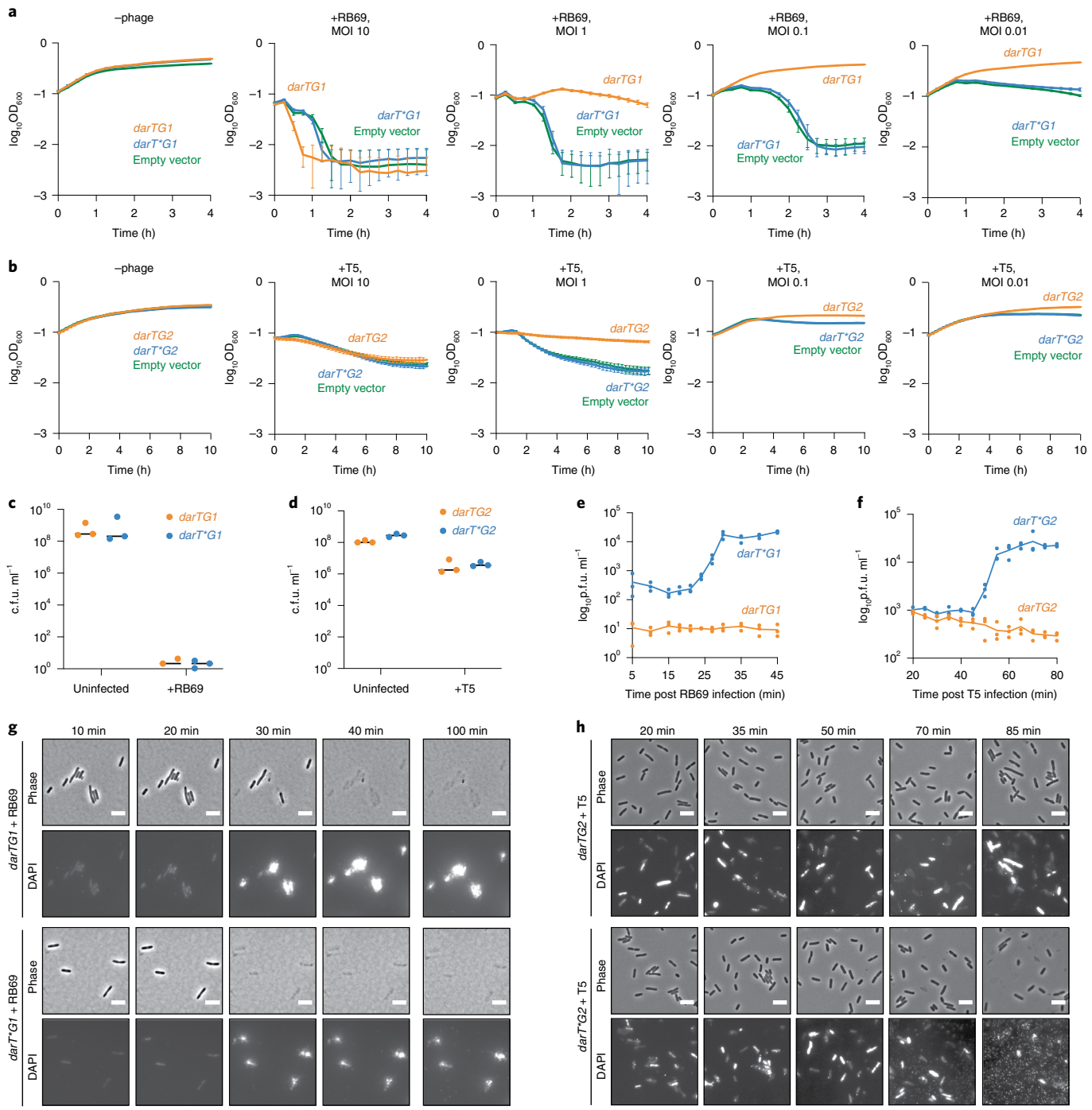

Fig. 2 | DarTG systems provide phage defence via an abortive infection mechanism. a,**b**, Growth curves for strains with an empty vector or the indicated plasmid-encoded TA system after infection with RB69 (**a**) or T5 (**b**) phage at varying MOI. The mean ± s.d. of 7–11 technical replicates are presented; data are representative of 2 independent experiments (Extended Data Fig. 3). **c**,**d**, Survival of *E. coli* encoding the indicated DarTG systems as measured by colony forming units (c.f.u.) after 15 min of infection with RB69 at MOI 5 (**c**) or 30 min of infection with T5 at MOI 20 (**d**). Data are from 3 independent biological replicates. **e**,**f**, One-step growth curves showing measurements of plaque forming units (p.f.u.) over time in cultures of DarTG1 or DarT*G1-containing cells infected with RB69 (**e**) or DarTG2 or DarT*G2-containing cells infected with T5 (**f**) at MOI 0.01 during the first round of infection. Data are from 3 independent biological replicates. **g**, Time-lapse microscopy of DAPI-stained RB69-infected *E. coli* encoding the indicated DarTG1 systems. Scale bars, 4 μM. **h**, Time-course microscopy of DAPI-stained T5-infected *E. coli* bearing plasmids with the indicated DarTG2 systems. The 85 min timepoint of DarT*G2 DAPI is displayed at a different scale to accommodate the high intensity of DAPI staining present in this sample. Scale bars, 4 μM.

or the artificial depletion of DarG, inhibits DNA replication in *E. coli* and *M. tuberculosis*[17,18,20]. However, we hypothesized that after phage infection, its more relevant biological function is to prevent the replication of phage genomes. To test this hypothesis, we first monitored the uptake of radiolabelled thymidine at various time points after RB69 infection. In DarTG1-containing cells, DNA synthesis rates did not substantially increase, particularly compared with cells with DarT*G1 where the levels of thymidine incorporation increased

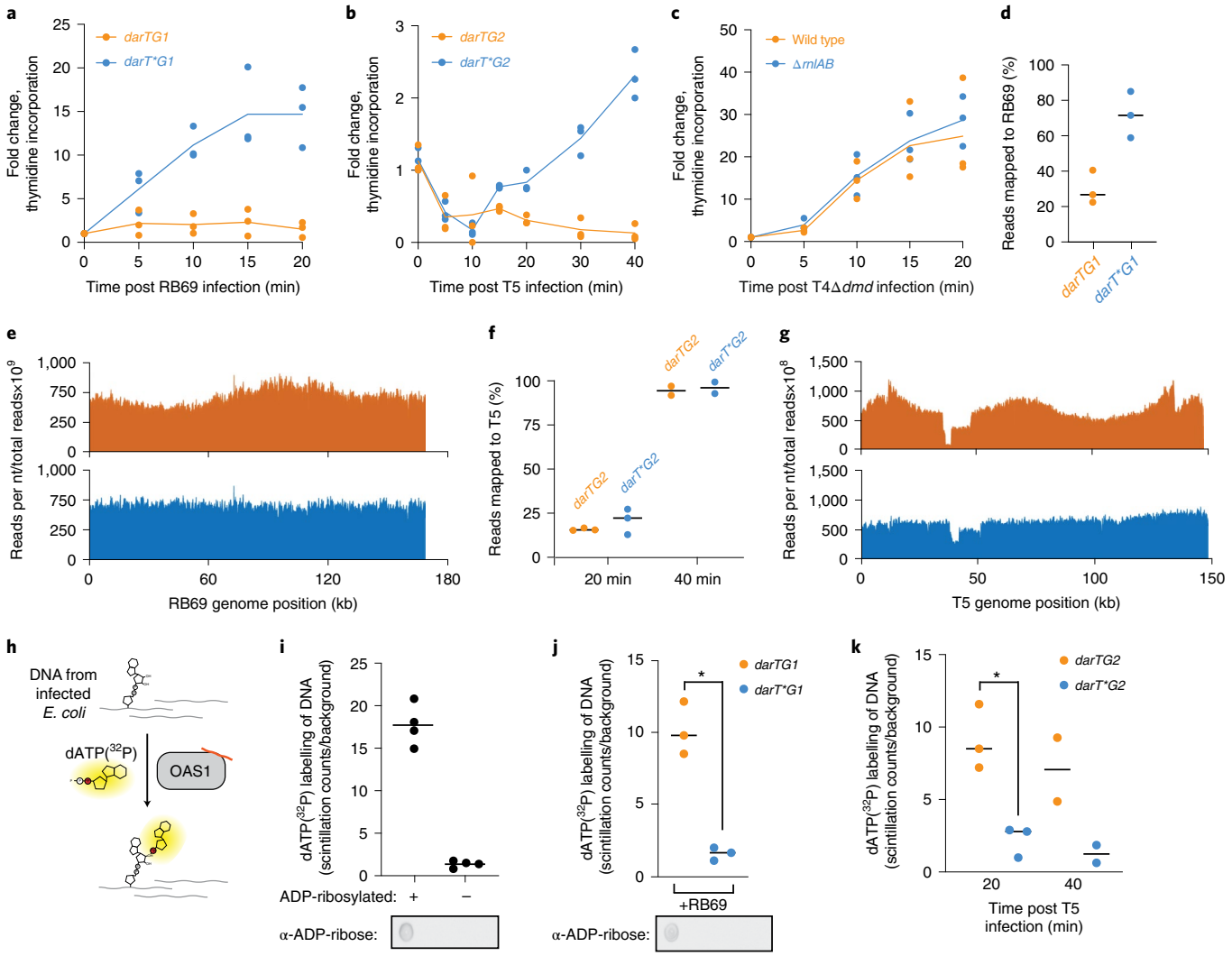

Fig. 3 | DarTG inhibits phage DNA replication by ADP-ribosylating viral DNA. a–**c**, DNA synthesis rates as measured by ^{3}H-labelled thymidine incorporation at the indicated time points after infection of strains encoding the indicated TA systems infected with RB69 at MOI 5 (**a**), T5 at MOI 20 (**b**) or T4 Δ*dmd* at MOI 5 (**c**). Graph depicts 3 independent biological replicates. **d**, Fraction of RB69 phage versus host-derived DNA, as determined by Illumina sequencing, for DNA extracted from DarTG1 or DarT*G1 cells infected with RB69 at an MOI of 5. Black lines indicate mean values. **e**, Sequencing read coverage from experiment in **d**. One representative sample is shown. **f**,**g**, Same as **d** and **e** but for T5 infection of DarTG2 and DarT*G2 cells at an MOI of 20. **h**, Overview of an ELTA assay, wherein DNA extracted from infected *E. coli* cells is incubated with OAS1 protein activated with the synthetic double stranded RNA analogue poly(I:C) (orange line) and ^{32}P-dATP. Incorporation of ^{32}P-dATP onto ADP-ribose modifications is measured by scintillation counting. **i**, ELTA measurements (top) and dot blots with an anti-ADP-ribose antibody (bottom) for an ssDNA fragment ADP-ribosylated in vitro compared to unribosylated DNA extracted from *E. coli*. Data from 4 independent replicates are shown. **j**,**k**, ELTA measurements of DNA from *E. coli* encoding the indicated DarTG systems after infection with RB69 at MOI = 5 and 15 min post infection (**j**) or T5 at MOI = 20 at 20 or 40 min post infection (**k**). *$P < 0.01$ (two-sided *t*-test). Bottom panel of **j** depicts a dot blot of corresponding DNA (DarTG1 cells, left; DarT*G1 cells, right) probed as in **i**. Each dot on the graph represents an independent biological replicate for ELTA assays, and the dot blots are representative of at least 2 independent experiments.

~15-fold following phage infection (Fig. 3a). Differences in DNA synthesis rates were detected as early as 5 min post infection, indicating a rapid activation of the DarT1 toxin following phage infection. DarTG2 similarly prevented an increase in DNA synthesis following T5 infection (Fig. 3b). To rule out that these effects of DarTG1 and DarTG2 were simply non-specific, or secondary, effects of an activated phage defence system, we also measured DNA synthesis rates in conditions where the *E. coli* RnlAB TA system, which contains an RNase toxin, is activated. We infected either wild-type or Δ*rnlAB* cells with T4 Δ*dmd*, a variant of T4 susceptible to defence by the RnlAB system[24]. The rate of DNA synthesis was similar in wild-type and Δ*rnlAB* cells, supporting the conclusion that DarTG1 and DarTG2 specifically affect phage replication (Fig. 3c).

We also deep sequenced DNA extracted from cells post infection. For RB69 infection of cells harbouring DarTG1, ~30% of the total DNA was phage derived, whereas for cells with DarT*G1, phage DNA was ~70% of the total (Fig. 3d). Taken together with the thymidine incorporation result for RB69 infections (Fig. 3a), this result indicates that active DarT1 prevents the replication and accumulation of new phage DNA. We also examined sequencing coverage across the RB69 genome, finding a non-uniform distribution of reads for cells with DarTG1, but not DarT*G1, suggesting that the toxin disrupts DNA replication elongation, not initiation (Fig. 3e).

For DarTG2 cells infected with T5, DNA sequencing indicated that only ~20% of reads were phage derived at 20 min post infection, but >90% of reads were viral by 40 min (Fig. 3f). There were no

major differences in the percentage of reads derived from T5 when comparing the DarTG2 and DarT*G2 cells, probably because T5 triggers rapid and complete degradation of the host chromosome in both cases[25]. Nevertheless, the thymidine incorporation assays indicated that phage replication was strongly inhibited in DarTG2 cells (Fig. 3b). Consistent with this interpretation, agarose gel electrophoresis of DNA extracted from infected cells demonstrated a substantial decrease in the total amount of DNA in DarTG2 cells compared with DarT*G2 cells (Extended Data Fig. 5). From the DNA sequencing we found that, as with DarTG1, there were also differences in read coverage indicating that DarT2 probably also disrupts phage DNA replication elongation (Fig. 3g). These results are consistent with an Abi mechanism in which the primary target of DarT is phage DNA, not host DNA.

DarT family toxins have been shown to ADP-ribosylate ssDNA in vitro and when overexpressed in bacterial cells[17]. We therefore hypothesized that RB69 and T5 infection activates the DarT1 and DarT2 toxins, respectively, and that activated toxin blocks replication of the phage genome by ADP-ribosylating DNA in the cell. To assess whether DarTG-dependent ADP-ribosylation of DNA occurs in vivo following phage infection, we adapted a recently developed technique for measuring ADP-ribosylation of proteins to measure ADP-ribosylation of DNA. This assay termed enzymatic labelling of terminal ADP-ribose (ELTA) leverages the enzymatic activity of the innate immune protein, OAS1, to covalently attach dATP to ADP-ribose moieties[26] (Fig. 3h). This assay has not previously been used to assess the ADP-ribosylation of DNA. Therefore, we first confirmed that purified ADP-ribosylated ssDNA produced robust signal in an ELTA assay (Fig. 3i). We also confirmed ADP-ribosylation in a dot blot using an antibody recently shown to specifically detect ADP-ribose modifications on DNA (Fig. 3i, bottom)[19].

We infected cells harbouring *darTG1* or *darT*G1* with RB69, isolated DNA and then added OAS1 and ^{32}P-dATP to label ADP-ribose groups on the DNA (Fig. 3h). We detected a 6.5-fold increase in ADP-ribosylation of DNA extracted from DarTG1-containing cells 20 min post infection compared with cells containing the inactive DarT1* variant by ELTA (Fig. 3j). We also detected a robust signal in an anti-ADP-ribose dot blot on the DNA extracted from RB69-infected cells containing DarTG1, but no signal for an equal amount of DNA extracted from infected cells harbouring DarT*G1 (Fig. 3j, bottom). In addition, we measured ADP-ribosylation of DNA following T5 infection of cells harbouring *darTG2* and found a similar, 3.5-fold increase in ADP-ribosylation in DarTG2 vs DarT*G2-containing cells after 20 min of infection (Fig. 3k). We also observed a ~5.7-fold increase in ADP-ribosylation of DNA after 40 min of infection when our sequencing indicated that virtually all DNA was of phage origin (Fig. 3f,k). Taken all together, our results indicate that DarT toxins are rapidly activated following phage infection and ADP-ribosylate phage DNA to disrupt its replication.

DarT blocks RNA synthesis and alters phage protein production. We also asked whether the DarTG systems impact RNA and protein synthesis. RNA synthesis rates were assayed by monitoring radiolabelled uridine uptake following infection. RNA synthesis was substantially reduced in both DarTG1 and DarTG2-containing cells following infection with RB69 and T5, respectively (Fig. 4a,b). To assess how DarTG1 and DarTG2 affect protein synthesis, we pulse-labelled cells pre and post infection and then measured the incorporation of radiolabelled cysteine and methionine using SDS–PAGE to resolve individual proteins. In contrast to DNA and RNA synthesis, protein synthesis rates did not differ substantially between DarTG1 and DarT*G1-containing cells infected with RB69 (Fig. 4c). However, there was a shift in which proteins were being synthesized, starting around 10 min post infection. In particular, late-appearing species in DarT*G1-infected cells (Fig. 4c) or empty vector-infected cells (Extended Data Fig. 6a) were either not seen or were substantially reduced in DarTG1-infected cells, with many early-appearing species persisting throughout the 20 min time course. In contrast, when transcription was shut off by treatment of cells with rifampicin, there was no shift in which proteins were being produced, only a reduction in band intensity (Extended Data Fig. 6b). Together, these results demonstrate that phage infecting cells containing DarTG1 can initiate their gene expression programme, but do not progress normally to the production of late gene products.

For DarTG2 and DarT*G2-containing cells infected with T5, the overall protein synthesis rates were again not substantially different (Fig. 4d). However, in this case, the banding pattern of DarTG2 and DarT*G2 cells remained more similar throughout the 40 min time course, although at the latest time points, DarTG2 cells appear to still be producing more middle gene products and less late gene products, as with DarTG1. Taken together, our results indicate that upon phage infection, both DarT toxins rapidly block DNA synthesis and reduce RNA synthesis. Protein synthesis rates are not substantially affected, but the timing and identities of proteins synthesized are misregulated. We conclude that DarT activation disrupts the proper development of mature virions. Even if phage capsids were produced, the inhibition of DNA synthesis (Fig. 3) means no new phage genomes are available for packaging.

RB69 can escape DarTG1 defence by mutating *61.2* (*adfA*). To gain additional insight into how DarTG systems function, we asked how phages can evolve to escape or overcome DarTG-mediated defence. To evolve resistant populations of phage, we serially passaged RB69 on both DarTG1 and DarT*G1-containing cells and monitored the pooled phage population for changes in susceptibility to DarTG1 (Fig. 5a)[27]. By pooling together phages propagated on cells containing DarT*G1, we were able to increase the diversity of the population, which cannot normally replicate on DarTG1-containing cells. We isolated a DarTG1-resistant clone from each of five different, independently evolved populations (Fig. 5b) and sequenced their genomes. We also evolved, in parallel as a control, a population of RB69 on only DarT*G1-containing cells and sequenced the genome of this population. We then identified mutations present in the DarTG1-resistant populations but not in the control population. For one clone, we could not identify any mutations, but the other four DarTG1-resistant clones each had a mutation in the same codon of the uncharacterized gene *61.2*, which is predicted to encode a 212 amino acid protein. In three cases, the mutation results in a substitution of arginine-164 with a histidine, while in the fourth, arginine-164 becomes a serine (Fig. 5b).

Intriguingly, a multiple sequence alignment of gp61.2 homologues, which are encoded in both phage and bacterial genomes, revealed that histidine and serine, as well as asparagine, occur naturally at this position (Fig. 5c). Two phages (T4 and T6) closely related to RB69 both encode homologues of gp61.2 containing a histidine at this position of gp61.2. Additionally, we noted that *61.2* is close within the RB69 genome to *dmd*, which encodes an inhibitor of the RnlA toxin of the RnlAB toxin-antitoxin system[24]. Together, these observations suggest that *61.2* homologues encode inhibitors of DarT toxins, with the identity of position 164 strongly influencing the specificity of inhibition. To test our hypothesis, we asked whether the ectopic production of gp61.2(R164H) from evolved RB69 or the gp61.2 homologue from T4 could restore the ability of wild-type RB69 to infect cells containing DarTG1 on the chromosome. Indeed, producing either of these constructs improved the efficiency of plaquing (EOP) of RB69 compared with cells harbouring an empty vector or producing the wild-type gp61.2 from RB69 (Fig. 5d). We also assessed DarT1 toxin activity when cells were infected with evolved RB69 phages by measuring DNA ADP-ribosylation levels, reasoning that if DarT1 is inhibited

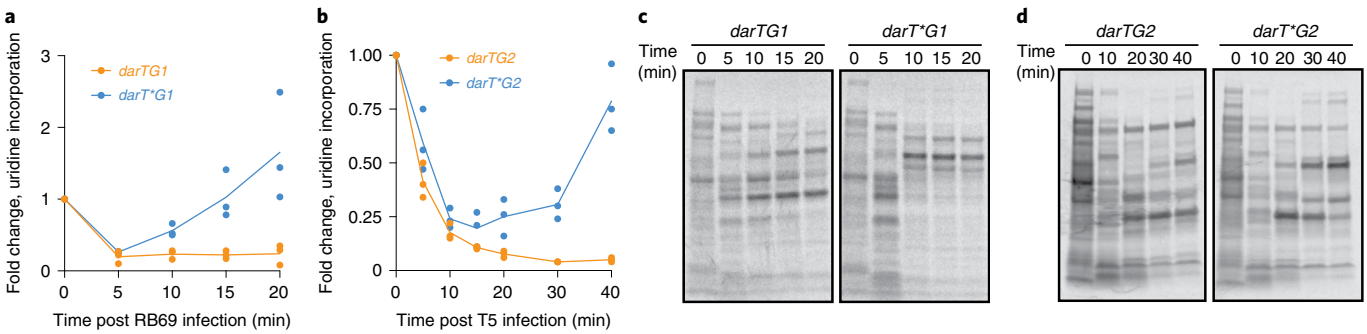

Fig. 4 | Activated DarT inhibits RNA synthesis and the timing of phage protein production. a,**b**, RNA synthesis rates as measured by ^{3}H-labelled uridine incorporation at various time points after infection of strains encoding the indicated TA systems infected with RB69 at MOI 5 (**a**) or T5 at MOI 20 (**b**). **c**,**d**, Protein synthesis rates as measured by ^{35}S-labelled cysteine and methionine incorporation at various time points after infection for *E. coli* encoding the indicated TA systems and infected with either RB69 at MOI 5 (**c**) or T5 at MOI 20 (**d**) and resolved by SDS–PAGE. Data shown are representative of 2 independent biological replicates.

by the gp61.2(R164H) variant, the toxin should be unable to ADP-ribosylate DNA. Consistent with this idea, there was no detectable DNA ADP-ribosylation in cells infected with the evolved RB69 producing the gp61.2(R164H) variant (Fig. 5e). We also tested whether the evolved gp61.2 could inhibit DarT1 in the absence of phage. Indeed, the gp61.2(R164H) variant, but not the wild-type gp61.2, could restore growth to cells producing DarT1 (Fig. 5f). Finally, we reasoned that a DarT1 inhibitor should not be essential to phage in the absence of *darTG1*. Using T4, which is amenable to genetic manipulation, we successfully made phage in which *61.2* contained a premature stop codon or had a large region deleted, and found that in both cases, the phages had no deficiency in plaquing on cells lacking *darTG1* (Extended Data Fig. 7). Taken all together, these data suggest that *61.2* encodes a DarT inhibitor and that the escape mutants we isolated improve the ability of the RB69 gp61.2 to inhibit DarT1. On the basis of these results, we have renamed *61.2* as *adfA* for anti-DarT factor A.

SECϕ18 can escape DarTG2 defence by mutating DNA polymerase. We also tried to evolve T5 phages to escape DarTG2-mediated defence, but were unable to identify escape mutants, even after several independent populations were passaged for 15 cycles each. We therefore tried to evolve SECϕ18 phage, which DarTG2 also defended against (Fig. 1a). In this case, resistant SECϕ18 populations were readily obtained, with increased infectivity emerging after 5 rounds of passaging (Fig. 5g). Full genome sequencing of the evolved escape phage populations and a control population passaged only on cells containing DarT*G2 revealed that each resistant population had accumulated one of five different mutations in *mga47*, which encodes the SECϕ18 DNA polymerase (Fig. 5g). The mutations in DNA polymerase did not obviously cluster when mapped onto a homology-modelled structure of the protein.

There are three possibilities for how these mutations allow SECϕ18 phages to escape the DarTG2 system: (1) SECϕ18 DNA polymerase normally activates the toxin, with the mutant variant having lost the ability to do so; (2) the mutant, but not wild-type, variant of DNA polymerase neutralizes the toxin; or (3) the mutant DNA polymerase overcomes or somehow circumvents the activity of the toxin. We ruled out possibility 1 by overexpressing *mga47* in cells containing the DarTG2 system and found that it did not induce toxicity, indicating that *mga47* is not sufficient to activate DarT2 (Fig. 5h). We addressed possibilities (2) and (3) by asking whether the DarT2 toxin was still able to ADP-ribosylate DNA following infection with the SECϕ18 escape phage. If ADP-ribosylation of DNA still occurs in the presence of the evolved phage, it would indicate that the DarT2 toxin is still active but that phages can replicate despite its activity. Indeed, we found that ADP-ribosylation of DNA occurs at a rate similar to that seen with wild-type SECϕ18 (Fig. 5i). This contrasts with what we had observed when evolved RB69 infected DarTG1 cells (Fig. 5e), further underscoring that these phages have overcome DarTG-mediated defence by different mechanisms. These results strongly support a model in which SECϕ18 modifies its DNA polymerase to accommodate the ADP-ribose modifications on the DNA made by DarT2.

Discussion

DarTG-based phage defence. Like most TA systems, the DarTG system had previously only been characterized through the artificial overexpression of DarT toxin or the depletion of its antitoxin[17,18,20]. This previous work elucidated the biochemical function of DarT toxins as ADP-ribosyltransferases that specifically target DNA and demonstrated that cells lacking DarG mount a DNA damage response as the ADP-ribosylation of DNA by DarT probably leads to replication fork stalling[23]. However, the physiological function and native triggers of DarTG systems have been unclear. A *Mycobacterium tuberculosis* strain lacking *darTG* was reported to have a modest increase in growth after 15 d, although whether the growth defect of the wild type results from ADP-ribosylation of DNA was not shown and why cells harbour a system that slows growth is not obvious. Here we demonstrated that DarTG1 and DarTG2, taken from two strains of *E. coli* and representing the two different major classes of DarTG systems, can provide host cells with potent defence against phages (Fig. 1).

The identification of phages that trigger these DarTG systems enabled us to characterize the activity of the toxins in vivo under growth conditions that naturally, and rapidly, liberate them. Our results indicate that within minutes after phages adsorb to the cell and inject their DNA, DarT toxins are active (Fig. 6). The liberated DarT then ADP-ribosylates phage DNA leading to a near complete cessation of DNA synthesis and an inhibition of RNA synthesis. These effects of the DarT toxins also impacted the programme of phage gene expression and limited the production of late proteins (Fig. 4). Even if procapsids did assemble, DNA packaging would not occur as the phage genome is not fully replicated in cells with active DarT. Our results indicate that DarTG functions through an Abi-like mechanism in which infected cells die, but without producing progeny phage, thereby sparing uninfected neighbour cells. Although DarT can also target the host cell's chromosome and is toxic when overexpressed, T5 and probably RB69 trigger chromosome degradation so there is probably little host DNA present for DarT to modify[28,29]. Even though the DarT toxin primarily targets viral DNA,

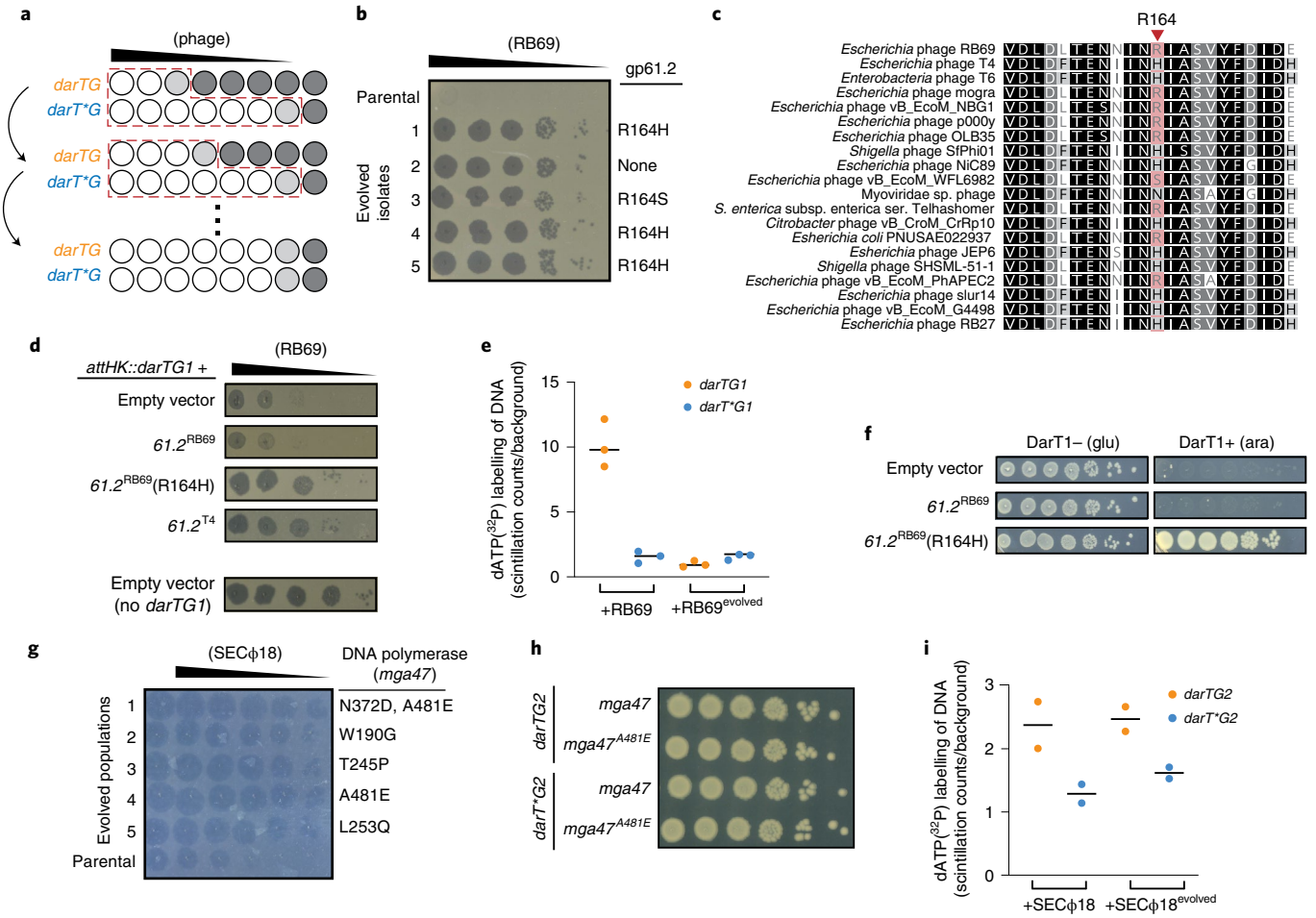

Fig. 5 | RB69 and SECϕ18 escape DarTG-mediated defence by two distinct mechanisms. a, Overview of phage evolution experiment. DarTG and DarT*G-producing cells seeded in 96-well plates were infected with 10-fold serial dilutions of phage, with the highest well infected at an MOI of ~10. Following incubation, all cleared and partially cleared wells (dashed red lines) were pooled and the resulting phages used to re-infect cells. This process was repeated until phage were able to clear an increasing number of wells of DarTG-containing cells. **b**, EOP of ancestral and evolved RB69 on DarTG1-containing cells. The mutations identified in gene *61.2* following genome sequencing are indicated on the right. The isolates shown were derived from 6 independently evolved populations of RB69. **c**, Sequence alignment of the region surrounding residue 164 of gp61.2 for 20 homologues. **d**, EOP of wild-type RB69 on *E. coli attHK::darTG1* either bearing an empty vector or producing the wild-type RB69 gp61.2, the evolved RB69 gp61.2(R164H) or the wild-type T4 gp61.2. Bottom panel depicts wild-type MG1655 bearing an empty vector. Data are representative of 2 independent biological replicates. **e**, ELTA-based measurements of ADP-ribosylation of DNA extracted from *E. coli* encoding *darTG1* or *darT*G1* and infected with an evolved RB69 clone. Data of wild-type RB69 infection (Fig. 3j) is reproduced here for comparison. Data are from 3 independent biological replicates. Black lines indicate mean values. **f**, C.f.u. measured in cells bearing a vector with DarT1 either repressed (+glucose (glu)) or induced (+arabinose (ara)) along with an empty vector, a vector expressing the wild-type RB69 *61.2* or the evolved RB69 *61.2(R164H)* variant. **g**, Plaque assays showing the increased resistance of 5 independently evolved populations of SECϕ18 selected to overcome DarTG2 defence, with the mutations identified by whole-genome sequencing of each population. **h**, Expression of the wild-type and an evolved allele of *mga47* gene in cells containing DarTG2 or DarT*G2. Data are representative of 2 independent biological replicates. **i**, ELTA-based measurements of ADP-ribosylation of DNA extracted from *E. coli* encoding *darTG2* or *darT*G2* and infected with the parental SECϕ18 strains or an evolved SECϕ18 clone. Data are from 2 independent biological replicates.

phage inhibition occurs after key phage processes (for example, chromosome degradation) have been initiated, hence the infected cells are unable to survive. Additionally, we isolated T5 escape mutants producing a variant phage DNA polymerase that enables replication of the phage genome despite its ADP-ribosylation by DarT and the subsequent release of mature virions. If DarT were aborting infection by modifying the host chromosome, such mutant phages would still be inhibited and not escape DarTG. Thus, we conclude that DarTG does not ultimately kill the host cell as in a conventional Abi mechanism, but instead acts to thwart phage replication directly.

Activation of the DarTG system by phage infection. How DarT becomes activated following phage infection is not yet clear. As noted above, DarT is active within 5 min post infection, as measured by differences in DNA synthesis rates between DarTG and DarT*G cells (Fig. 3a), but without transcriptional induction of the system. Recent work on an *E. coli* ToxIN system demonstrated that the antitoxin *toxI* is intrinsically unstable and so must be continuously produced to bind and neutralize ToxN[13]. Phage-induced shutdown of host transcription following T4 infection leads to the liberation of ToxN, an endoribonuclease, ~20 min post infection. DarT activation could work similarly. However, although the antitoxins of TA systems are often more unstable than their cognate toxins, we recently found that many are not unstable enough to produce pools of active toxin on the timescale of a phage infection simply by blocking transcription[10]. Thus, we favour the possibility that

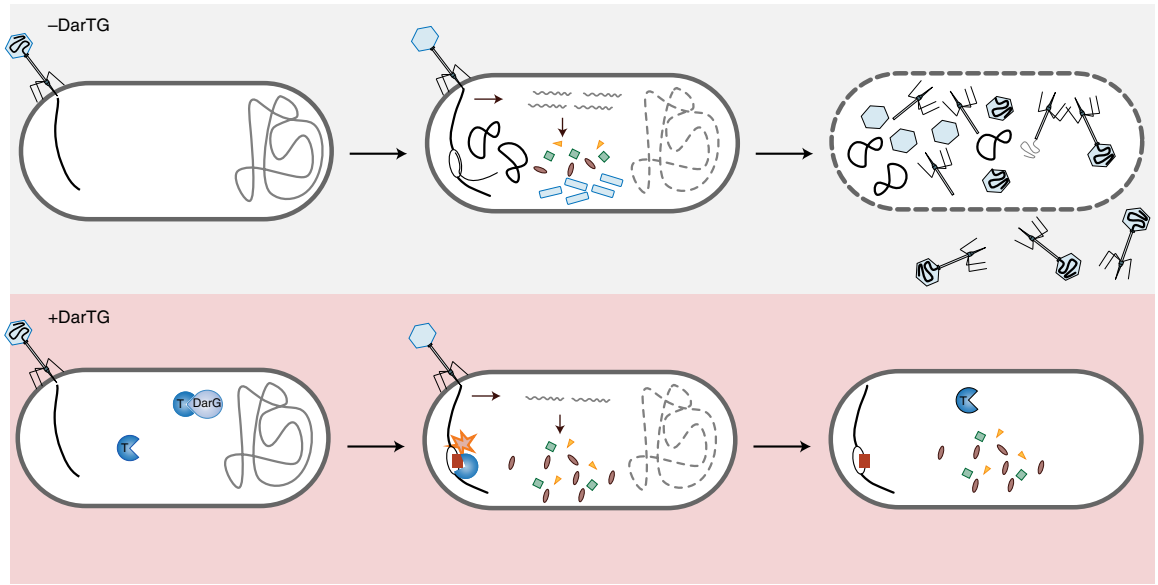

Fig. 6 | Model for DarTG-mediated defence against phage. When DarTG is not present (top), phage adsorb, inject their DNA and begin producing mRNAs and proteins. These proteins enable them to degrade the host chromosome, replicate their DNA and produce the structural components required to make new phage particles. These components are assembled into capsids into which newly replicated genomes are packaged before lysis of the host cell. When DarTG is present (bottom), phage infection triggers release of the DarT toxin. The toxin ADP-ribosylates phage DNA, thereby inhibiting DNA synthesis and reducing transcription. Because some transcription occurs, particularly early on, phage are able to degrade the host chromosome and the host cell does not recover. However, due to the absence of newly replicated phage genomes and reduced late protein production, new phage particles are not produced.

a particular phage protein or factor somehow triggers activation of DarT. The involvement of a specific phage protein would potentially explain why DarTG1 and DarTG2 protect against different phages (Fig. 1a) and it might also explain why different growth conditions are required for their activity. Activation may require particular growth conditions if a host factor, such as a chaperone or a protease, is required for releasing the toxin, but that factor is less abundant or less available in particular growth states.

If a specific phage protein is required to trigger DarT, it could stimulate separation of DarT from its cognate DarG antitoxin. However, the DarG antitoxins may not only bind and inhibit their cognate DarT toxins, as with canonical type II TA systems. Previous work on the enteropathogenic *E. coli* DarTG system indicated that these systems may also rely on a type IV mechanism in which the antitoxin indirectly antagonizes the toxin's activity[18]. Notably, DarG1 contains structural homology to a YbiA-like domain that is predicted to be an ADP-ribose processing enzyme and DarG2 contains a classic macrodomain typically associated with ADP-glycohydrolases known to remove ADP-ribose modifications[21,22]. Thus, in principle, DarT may always be active, but with sufficient DarG activity in uninfected cells to offset its toxicity. A phage product could inhibit, sequester or degrade DarG, enabling the rapid accumulation of DarT activity.

Phage evasion of DarTG-mediated defence. Phages and their hosts are locked in an arms race wherein hosts acquire or evolve protection from phage infection, and phages evolve mechanisms to overcome these defences. By evolving RB69 to escape the defence offered by DarTG1, we identified *adfA* (formerly *61.2*) as a probable phage-encoded anti-DarT factor. The AdfA encoded by RB69 probably enables this phage to inhibit a different, but closely related DarTG system. The single substitutions in AdfA we identified enabled RB69 to then overcome the DarTG1 system we introduced. Notably, the mutations selected for in AdfA convert arginine-164 to histidine or serine, which occur naturally at the equivalent position in some AdfA homologues. The presence of *adfA* homologues in T4, T6, RB69 and other T-even phages suggests that these phages have all been exposed to and selected to produce anti-DarT proteins, underscoring the notion that DarTG systems are critical and probably common phage defence systems in *E. coli* and possibly many other species. The *adfA* homologues are all found in similar genomic positions in the genomes of T-even phages and relatively close to *dmd* homologues that encode for RnlA toxin inhibitors. Thus, this region may represent an anti-TA system island, similar to the anti-CRISPR islands documented in mobile genetic elements of Enterobacteriaceae and *Pseudomonas*[30].

For SECϕ18, the mutants that escape defence by DarTG2 all harboured point mutations in *mga47*, which encodes the phage DNA polymerase (Fig. 5g). Our ELTA measurements indicated that the DNA of escape phages is ADP-ribosylated to a similar extent as wild-type phages (Fig. 5i), suggesting that the mutations in *mga47* are not leading to a disruption of DarT2 activity. These *mga47* mutations could, in principle, enable phage replication to happen faster and before DarT2 activity accumulates. More probably, they somehow promote the replication of modified DNA, but precisely how this occurs remains to be studied.

TA systems in phage defence. Our bioinformatic screen indicated that DarTG homologues are often found in phage defence islands and the initial report on DarTG noted that homologues are sometimes inserted within type I restriction-modification systems. These results further support the notion that proximity to known phage defence elements is a powerful means of identifying new phage defence systems[3,15,17]. Intriguingly, the RnlAB family, which is known to consist of phage defence systems RnlAB and LsoAB, had the lowest phage defence score measured[14,24] (Supplementary Table 1). This could indicate that only a subset of the RnlAB family is involved in phage defence. The two DarTG systems we examined are not encoded near any known or predicted phage defence system and instead are encoded within prophages (Fig. 1e). Previous work has found that prophages often harbour phage defence systems[31–33]. The presence of TA systems on prophages has also been

documented, and in some cases these systems may stabilize prophages within the bacterial chromosome, analogous to the role of some TA systems in stabilizing plasmids[34–36]. However, the primary, or perhaps additional function, of these prophage-associated TA systems may be to exclude other phage, which by threatening the host cell, also jeopardize their survival and propagation.

Identifying other TA systems that are associated with defence islands or encoded within prophages could help to identify additional systems that function in phage defence. These systems may provide cells with a diverse arsenal of anti-phage elements that complement restriction-modification and CRISPR systems. Importantly, these latter systems can only block phages by degrading phage DNA or RNA, whereas TA systems employ toxins with a wide range of enzymatic activities, including the DarT toxins we found here that ADP-ribosylate phage DNA.

Methods

Analysis of TA system association with defence islands. Protein sequences of all genes in a set of 38,167 bacterial and archaeal genomes were downloaded from the Integrated Microbial Genomes (IMG) database[37] in October 2017. These proteins were clustered using the 'cluster' option of MMseqs2 (release 2-1c7a89, ref. [38]), with default parameters. Clusters were further aggregated into larger clusters using four additional cycles of clustering; in each cycle, a representative sequence was taken from each cluster using the 'createsubdb' option of MMseqs2 and representative sequences were clustered using the 'cluster' option with the '–add-self-matches' parameter. For the first additional clustering cycle, the 'cluster' option was run with default parameters; for the additional cycles 2–4, clustering was run with sensitivity parameter '-s 7.5', and for the additional cycle 4, the '–cluster-mode 1' parameter was also added.

Each cluster with 20 or more genes was annotated with the most common protein families (pfam), clusters of orthologous genes (COG) and IMG product annotations in the cluster. For each toxin belonging to one of the analysed toxin families, genes from all clusters annotated as containing this toxin were aggregated. For each of the toxins families, the fraction of genes that have known defence genes in their genomic environment spanning 10 genes upstream and downstream of the inspected gene was recorded. Defence score for each toxin family was calculated as previously described, except that genes belonging to TA systems were eliminated from the positive set[3]. A representative DarTG system from two distinct families were identified in *E. coli* strains for further analysis: DarTG1 is encoded in *E. coli* C7 (accession number CP010240.1) and DarTG2 is encoded in *E. coli* 2-460-02_S4_C3 (accession number NZ_JNRF00000000.1).

Analysis of DarTG1 and DarTG2 context and sequence. A blastp search was seeded with either DarT1 or DarT2. Resulting hits with *e*-values $<10^{-50}$ were selected, and associated nucleotide sequences were obtained. Prophage regions were identified as those with >50% of genes having annotated phage elements (for example, genes predicted to encode integrases, recombinases, phage tail or phage capsid proteins) or by using the Phaster phage identification web tool (www.phaster.ca). Phage defence elements were identified by referencing Genbank annotations with known phage defence systems (for example, restriction-modification, abortive infection).

Representative examples of DarTG1 systems were identified through a blastp search seeded with DarG1 with *e*-values $<10^{-50}$. Because of conserved gene order (*darT* always preceding *darG*), the protein sequence of the protein upstream was used for the DarT alignments. For DarTG2, systems were identified from previous studies[17,18,20], or through a similar strategy described for DarTG1. Protein sequences were aligned in Geneious v. 2020.0 (Biomatters) using the Clustal Omega algorithm and the resulting image files were exported. Similarity was determined using a Blosum62 matrix with threshold set to 1. In each column, the largest group of similar residues was identified and coloured according to the indicated legend; any residues outside of this group are not coloured. Annotations for DarG protein domains were identified through a BLAST (macrodomain) or Phyre2 structural prediction (YbiA-like, 80% confidence).

Strains and growth conditions. All bacterial and phage strains are listed in Supplementary Table 2. *E. coli* was grown at 37 °C in LB medium for routine maintenance and cloning. Phages were propagated by infecting *E. coli* MG1655 or *E. coli* MG1655 Δ*rnlAB* (T4 Δ*dmd* only) cultures of OD_{600} ~0.1–0.3 at an MOI of 0.1 and incubated with aeration at 37 °C. Following clearing, any remaining cells were pelleted by centrifugation and lysates were filtered through a 0.22 µM filter. SECϕ18 was concentrated for ELTA experiments by centrifugation of cleared lysates for 2 h at 10,000×*g* and resulting pellets were resuspended in ~100× less volume.

All RB69 infection experiments were performed at 37 °C in LB medium, whereas experiments with T5 and SECϕ18 were performed at 30 °C and 20 °C, respectively, in M9 medium (6.4 g l^{-1} Na_2HPO_4-$7H_2O$, 1.5 g l^{-1} KH_2PO_4, 0.25 g l^{-1} NaCl, 0.5 g l^{-1} NH_4Cl medium supplemented with 0.1% casamino acids, 0.4% glucose, 2 mM $MgSO_4$ and 0.1 mM $CaCl_2$). Overnight cultures were prepared in the same media used in the experiment. Media for selection or plasmid maintenance were supplemented with carbenicillin (100 µg ml^{-1}), chloramphenicol (20 µg ml^{-1}), kanamycin (30 µg ml^{-1}), or spectinomycin (100 µg ml^{-1}) as necessary unless otherwise indicated. Induction of ectopic expression were effected with anhydrous tetracycline (100 ng $µl^{-1}$), arabinose (0.2% w/v) or vanillate (100 µM) as necessary.

Plasmid construction. All primer and synthesized gene sequences are listed in Supplementary Table 3. DNA encoding candidate DarTG1 and DarTG2 system open reading frames, as well as 200 bp upstream and overlapping ends to the pBR322 vector (MLR1 and MLR2, respectively), were commercially synthesized by Integrated DNA Technology as gBlocks and assembled into a promoter-less backbone of pBR322 amplified with primers MLR3 and MLR4 by Gibson assembly. The pBR322-DarTG1^{E152A} and pBR322-DarTG2E^{147A} variants were inserted into the corresponding wild-type plasmids by site-directed mutagenesis with inverse PCR using primers MLR5 and MLR6, or MLR7 and MLR8, respectively. To generate the chromosomal insertion of *darTG1*, the *darTG1* region containing its native promoter was amplified with primers MLR9 and MLR10, and cloned into pAH144 vector linearized with primers MLR11 and MLR12 by Gibson assembly. The *mga47* open reading frame was amplified from wild-type or evolved SECϕ18 with primers MLR13 and MLR14, and cloned via Gibson assembly into a version of pBAD33 with a kanamycin resistance cassette linearized with MLR15 and MLR16. The *61.2* open reading frame was amplified from either the wild-type RB69 or an evolved clone from population 1 with primers MLR17 and MLR18, or from T4 phage with primers MLR19 and MLR20, and cloned into pKSV45-P_{van}-kan linearized with primers MLR21 and MLR22. The pEXT20-*61.2*^{RB69} and pEXT20-*61.2*^{RB69} (R164H) vectors were generated by Gibson assembly in which the pEXT20 vector was linearized with primers MLR29 and MLR30 and the insert was amplified from the wild-type RB69 DNA or the evolved phage using primers MLR31 and MLR32. The p-DarT1 construct, in which the toxin is expressed from an arabinose promoter, was produced by amplifying DarT1 using primers MLR33 and MLR34, digested with SacI and KpnI, and ligated into the pJB37 vector digested with the same enzymes[39]. All plasmids were confirmed by Sanger sequencing of the inserts.

Strain construction. Plasmids described above were introduced into MG1655 by TSS transformation or electroporation[40]. A single copy of *darTG1* was inserted onto the MG1655 chromosome at the HK022 attachment site using the CRIM system[41], employing the pAH144-*darTG1* vector with the pAH69 helper plasmid. A scarless unmarked deletion of *rnlAB* was constructed by two-step allelic exchange. The *sacB-neoR* cassette from pIB279 was amplified with ML23 and ML24 and inserted using lambda Red recombinase[42,43]. The deletion oligo (MLR25) was subsequently transformed into lambda Red-containing cells and counterselection was performed on 5% sucrose plates. The deletion of *rnlAB* was verified by PCR amplification and sequencing of sucrose-sensitive, kanamycin-sensitive clones.

Phage gene deletions. T4 mutants were generated using a CRISPR-Cas system for targeted mutagenesis[44]. Sequences for RNA guides to target Cas9-mediated cleavage were designed using the toolbox in Geneious Prime 2021.2.2 targeting *adfA* but nowhere else in the T4 genome. The guides were inserted into the pCas9 plasmid as previously described[45] using oligos MLR27 and MLR28, and the resulting pCas9-*61.2*-cr6 plasmid was transformed into MG1655 and tested for its ability to target the T4 genome by restricting T4. Escape plaques were isolated, and two mutated variants with disruptions of the *61.2* gene were identified by sequencing a premature stop codon at position 68 and a large deletion of residues 65–196 (Extended Data Fig. 7).

Plaque assays, phage titering and efficiency of plating assays. Overnight cultures of the indicated bacterial cells were mixed 1:200 with melted 0.5% agar made with either LB or M9 medium. The agar was then overlaid onto a 1.2% agar plate composed of the corresponding medium. Tenfold serial dilutions of the indicated phage were spotted on top. For RB69 experiments, plates composed of LB medium were incubated at 37 °C, whereas for T5 and SECϕ18 experiments, plates were composed of M9 medium and incubated at 30 °C and 20 °C, respectively. All experiments were performed independently at least three times.

Growth curves. *E. coli* bearing the indicated DarTG plasmids were grown to an OD_{600} of 0.3 and then mixed with phages at the indicated MOIs. Replicate (8–12) 100 µl aliquots of the resulting mixtures were seeded into 96-well plates, and growth was measured at 15 min intervals, with orbital shaking on a plate reader (Biotek) at 37 °C for DarTG1-RB69 experiments and 30 °C for DarTG2-T5 experiments. Outliers were removed and data presented are the mean and standard deviation of 6–12 plate replicates. Experiments were replicated independently at least two times.

Bacterial survival after phage infection. *E. coli* MG1655 containing either DarTG1 plasmids (pBR322-*darTG1* or *pBR322-darTG1*) or DarTG2 plasmids (pMLR6, pMLR7) were grown to OD_{600} of 0.3 and then phages were added at an MOI of 5 for the RB69 experiments and MOI of 20 for the T5 experiments. Suspensions were incubated without shaking for 5 min to allow for adsorption,

then cultures were washed twice with an equal volume of media to remove unadsorbed phage. Infected cells were incubated at the appropriate temperatures for an additional 5–10 min before serial dilutions were plated onto LB plates to determine bacterial colony forming units (c.f.u.). Data presented are the mean and standard deviation of 3 independent biological replicates.

One-step growth curves. Bacterial cells with appropriate plasmids were infected at an MOI of 0.01 in LB medium at 37 °C (*darTG1*-RB69 experiment and *rnlAB*-T4Δ*dmd* experiment) or in M9 medium at 30 °C (*darTG2*-T5 experiment). Samples were collected at regular time intervals, serially diluted and immediately spotted onto 0.5% LB top agar mixed with a wild-type MG1655 indicator strain to determine plaque forming units (p.f.u.) per ml. Data presented are the mean and standard deviation of 3 independent biological replicates.

Microscopy. Cells were grown under conditions described above to an OD_{600} of 0.3, then stained with DAPI (1 μg ml^{-1}) for 10 min. Cells were then treated with 100 μg ml^{-1} carbenicillin or infected with phages at an MOI of 5 (RB69) or 20 (T5), as indicated in figure legends. For *darTG1*-RB69 experiments, the resulting suspension was washed once to remove unadsorbed phages and 1 μl was spotted onto a 1.5% agarose pad prepared with LB containing DAPI (1 μg ml^{-1}) and placed in a 35 mm glass-bottom dish with 20 mm microwell #0 coverglass (Cellvis) sealed with parafilm. Phase-contrast and epifluorescence images were taken at 10 min intervals using a Hamamatsu Orca Flash 4.0 camera on a Zeiss Observer Z1 microscope using a ×100/1.4 oil immersion objective and an LED-based Colibri illumination system using MetaMorph software (Molecular Devices).

For *darTG2* experiments, the DAPI-stained infected cells were incubated with shaking at 30 °C and 1 ml aliquots were removed at the indicated time points. Cells were washed once to remove unadsorbed phage, spotted onto 1.5% agarose pads prepared with M9 medium, placed on glass slides, and 3–5 fields were immediately imaged. Data presented are representative of at least 2 independent biological replicates.

Representative cells from the 20 min timepoint of the DarTG1 and DarT*G1 datasets were analysed in Fiji using the 'Plot Profile' tool and the measurements were normalized to cell length. Each cell profile was smoothed in Excel using the 'Exponential Smoothing' tool with a damping factor of 0.7. Fluorescence profiles were visually inspected and categorized into diffuse, asymmetric and bimodal groups.

DNA extractions after phage infection. For bulk DNA assays, cells in a volume of 10–25 ml were grown and infected as described above for bacterial survival assays, and were incubated with aeration until the indicated time points. One millilitre of the bacterial culture was pelleted and washed once to remove unadsorbed phage. DNA used for sequencing and ELTA experiments were derived from 10 ml of culture collected by vacuum filtration onto a 0.2 μM filter and washed once with an equal volume of media. Filters were placed in conical tubes and cells were removed by scraping into 1 ml of media and pelleting the resulting suspension. In all experiments, samples were flash frozen in liquid nitrogen and stored at −80 °C. DNA was extracted using the Gentra Puregene kit (Qiagen). For agarose gels, an equal volume of DNA was loaded for each sample and visualized on a 0.7% agarose gel stained with ethidium bromide. The amount of DNA was quantified in Fiji (http://imagej.nih.gov/).

Incorporation assays. Bacterial cells were infected under the same conditions as described for bacterial survival assays and flasks were maintained with aeration at the appropriate temperature. For DNA and RNA synthesis measurements, an aliquot of the bacterial culture was removed before phage addition ($T=0$ min) or at the indicated time points post infection, and transferred to a microcentrifuge tube containing methyl-^{3}H thymidine (Perkin Elmer) (40 μCi ml^{-1}) or uridine, 5-6(^{3}H) (Perkin Elmer) (6 μCi ml^{-1}). Tubes were incubated at the same temperature as infected cultures for 1 min (37 °C growth) or 2 min (30 °C growth). Reactions were quenched by addition of non-radioactive thymidine or uridine (1.5 mM) and incubated an additional 1 or 2 min. Samples were added to ice-cold trichloroacetic acid (TCA) (10% w/v) and incubated at least 30 min on ice to allow precipitation. The resulting sample was vacuum filtered onto a glass microfibre filter (Whatman, 1820-024) that had been pre-wetted with 5% w/v TCA. Filters were washed with 35x volume of 5% w/v TCA, then with 5x volume of 100% ethanol. Air-dried filters were placed in tubes with scintillation fluid and measured in a scintillation counter (Perkin Elmer). Three independent biological replicates are presented.

For protein synthesis assays, a 1 ml aliquot of bacterial culture was removed either before phage addition or rifampicin treatment ($T=0$ min), or at indicated time points post treatment, and incubated with EasyTag EXPRESS-^{35}S protein labelling mix, (^{35}S) (Perkin Elmer) at 44 μCi ml^{-1} for 2 min (37 °C) or 10 min (30 °C). Labelling was quenched with addition of unlabelled cysteine and methionine at 3 mM, and proteins were precipitated by addition of ice-cold TCA (13% w/v) and incubation on ice for at least 30 min. Samples were pelleted, washed twice with 100% acetone, then resuspended in resuspension buffer (100 mM Tris (pH 11.0), 3% w/v SDS). Samples were resolved by 4–20% SDS–PAGE, after which the gel was soaked in Gel Dry drying solution (Thermo Fisher), dried on a vacuum dry gel dryer and exposed to a phosphorimaging screen for 1–4 d. The screen was imaged on a Typhoon scanner (GE Healthcare) at 50 μM resolution. A representative image of two independent experiments is presented.

DNA sequencing. DNA collected as described above was sheared in a Diagenode Bioruptor 300 sonicator water bath for 15 ×10 s cycles at maximum intensity. Samples were further purified with a Zymo PCR cleanup kit and concentrations were determined on a Nanodrop. Sequencing libraries were prepared by shearing DNA to 150–200 nt using a Bioruptor (Diagenon), then cleaning and size-selecting DNA using AMpure XP magnetic beads (Beckman Coulter). The resulting DNA was end-repaired with T4 DNA polymerase (NEB), Klenow DNA polymerase (NEB) and T4 polynucleotide kinase (NEB), AMPure bead purified, then 3' adenylated using Klenow Fragment (3'-5' exo) (NEB). Adaptors were ligated with blunt/TA ligase master mix (NEB) and amplified with barcoding primers for ~10 cycles with KAPA Hi-Fi master mix (Roche). The resulting libraries were cleaned and size selected with Ampure XP beads, and run on a NextSeq500 at the MIT BioMicroCenter. Sequencing data are available at the NCBI Sequence Read Archive (BioProject PRJNA776027).

Reads were trimmed and mapped using Geneious 2020.0 (Biomatters) with the Geneious medium-sensitivity mapping to both MG1655 (accession number CP025268.1) and phage reference genomes (RB69 accession number NC_004928; T5 accession number NC_005859.1). The percent of reads mapping to the phage genome was calculated as (reads mapped to phage/total reads mapped × 100) for each sample and is the average of sequencing data generated from 2 or 3 independent biological replicates. Coverage maps were generated by dividing the number of non-end-gap characters at each position by the sum of all positions and multiplied by 10^{9}, then generating a moving average with an interval of 100. The resulting data were plotted as a function of position. Coverage data presented are from one replicate representative of 2–3 independent biological replicates.

ELTA assays. A positive control was generated in vitro via enzymatic ADP-ribosylation of ssDNA as described previously[17]. Briefly, a 10 μl reaction containing 30 ng μl^{-1} of DNA substrate containing a TCTC motif (MLR26), 50 mM Tris-HCl pH 8.0, 150 mM NaCl, 100 μM NAD^{+}, and 30 ng μl^{-1} recombinant *Taq* DarT (from *Thermus aquaticus*) was incubated at 37 °C for 2 h. The reaction was purified using the Monarch PCR and DNA cleanup kit (NEB) to remove unincorporated dATP. The successful incorporation of ADP-ribose was confirmed by visualization on 3% agarose gel after ELTA labelling with Cy5-dATP. The experiment in Fig. 3i was performed with 10 femtomole of the in vitro produced ADP-ribosylated DNA, while the control reaction with non-ribosylated DNA was performed using 1 μg of sheared DNA extracted from *E. coli* cells grown to mid-log phase.

DNA for all other ELTA assays was collected as described above. For SECϕ18 experiments in Fig. 5i, cells were infected at an MOI of 1,000 due to the low adsorption of this phage under the growth conditions (<1%) and infected cultures were incubated for 2 h before collection. The DNA was sheared for 15 ×30 s cycles on the BioRuptor sonicator on the maximal intensity setting and even shearing was confirmed by agarose gel electrophoresis. The resulting samples were further purified with a Zymo DNA Clean and Concentrator kit (Zymo Research).

Each 20 μl ELTA reaction consisted of 10 mM Tris-HCl pH 7.5, 20 mM magnesium acetate, 2.5 mM 1,4-dithiothreitol, 10 μCi (0.05 μCi μl^{-1}) dATP, α-^{32}P (Perkin Elmer), 2 μM OAS1, 100 μg ml^{-1} low molecular weight poly I:C (Invivogen) and 1 μg of DNA. These reactions were incubated at 37 °C for 2 h after which the DNA was purified as for the control DNA. Half of the resulting sample was transferred to a 4 ml scintillation tube and counted as above. Data were normalized to a reaction run with no DNA input. This ADP-ribosylated ssDNA control was run alongside each set of reactions to confirm normal assay function. Two or three independent biological replicates are presented in each graph.

Anti-ADP-ribose dot blots. Dot blots were performed as described previously[19]. A 2 pmol aliquot of either the ADP-ribosylated ssDNA substrate or the corresponding unribosylated substrate (described above) (Fig. 3i), or 2 μg of DNA isolated from phage-infected cells (either DarTG1 or DarT*G1-containing, as described above) (Fig. 3j), was spotted onto a nitrocellulose membrane and cross-linked at 1,200 J with a Stratalinker UV cross-linker. The membranes were probed with poly/mono-ADP-ribose antibody (E6F6A; Cell Signaling) at 1:1,000. Membranes were developed with SuperSignal West Femto maximum sensitivity substrate (Thermo Fisher) and imaged on a ChemiDoc system (Biorad). One blot is depicted, which is representative of two independent experiments.

Phage evolution experiments. Each RB69 evolution experiment consisted of 8 wells of cells producing DarTG1 (ML3) and 8 wells of cells producing DarT*G1 (ML4) seeded with ~10^{6} cells per well from overnight bacterial cultures in a 96-well plate in LB medium. Cells were infected with 10-fold serial dilutions of phage cultures with the highest MOI at 10, and one well of each strain was uninfected to control for cross-contamination. Plates were sealed with Breathe Easy plate seals (Sigma) and aerated by micro-orbital shaking in an ELMI plate shaker at 37 °C. Plates were incubated for 4–6 h. The cleared and partially cleared wells were pooled, centrifuged to remove unlysed bacteria, and the resulting supernatants were used to infect the next evolution round. Resistance to DarTG1 was monitored

by the number of cleared wells as well as by EOP assays. Once resistance to DarTG1 was observed, single plaques were isolated in top agar plates and tested for resistance. One resistant clone from each of 5 independently evolved phage populations was propagated for further analysis and sequencing as described below. A control population that was only passaged on cells containing DarT*G1 was also analysed.

The SECϕ18 evolution experiments were designed as above, except that wells were seeded with *E. coli* cells producing DarTG2 and DarT*G2, propagated in M9-glucose medium, and plates were incubated at 20 °C for 16 h. Sequencing was performed on evolved populations as opposed to single clones described for the RB69 evolution.

To extract phage DNA, lysed bacterial cultures were centrifuged to remove bacterial cells, then 100 µl of supernatant containing phages was incubated with TURBO DNase I (0.1 mg ml^{-1}) and RNase A (0.1 mg ml^{-1}) for 45 min at 37 °C to remove residual nucleic acids from bacterial cell lysis. Nucleases were inactivated by addition of EDTA (10 mM) and incubation for 15 min at 37 °C. Proteinase K (0.2 mg ml^{-1}) was added and samples incubated at 50 °C for 30 min to disrupt phage capsids. Samples were centrifuged for 2 min at 21,000 × *g* and DNA precipitated from the supernatant by standard sodium acetate/ethanol precipitation. The resulting DNA was processed for Illumina sequencing as described for *E. coli* infection sequencing experiments and mapped to the RB69 reference genome (NC_004928) or SECϕ18 reference genome (LT960609). Only mutations that arose uniquely in the phages evolved on *E. coli* containing DarTG, that were not also found in the phages evolved on *E. coli* lacking active DarTG systems, were considered. For the SECϕ18 control population, only the two genes (*mga32* and *mga47*) that had acquired mutations in the populations evolved in the presence of DarTG2, were PCR-amplified and Sanger sequenced. Mutations were also identified in *mga32* for the control experiment, so only *mga47* mutations were considered relevant to DarTG2 resistance. Mutations were identified using Geneious Variant Finder, with the threshold set to >20%.

Reporting summary. Further information on research design is available in the Nature Research Reporting Summary linked to this article.

Data availability

The bioinformatic analysis was performed using protein sequences available in the Integrated Microbial Genomes (IMG) database (https://img.jgi.doe.gov/). DarTG1 and DarTG2 were identified in *Escherichia coli* C7 (NCBI accession GCA_001901425.1) and *Escherichia coli* 2-460-02_S4_C3 (NCBI accession GCA_000704545.1). Sequencing data are available on NCBI (BioProject PRJNA776027). Sequencing data were aligned to reference genomes of MG1655 (accession number CP025268.1), RB69 (accession number NC_004928), SECϕ18 (accession number LT960609) or T5 (accession number NC_005859.1). All other source data have been deposited to Mendeley Data V1 at https://doi.org/10.17632/v9bmr549nf.1. Source data are provided with this paper.

Received: 19 October 2021; Accepted: 18 May 2022;
Published online: 20 June 2022

References

1. Bernheim, A. et al. Prokaryotic viperins produce diverse antiviral molecules. *Nature* **589**, 120–124 (2021).
2. Cohen, D. et al. Cyclic GMP-AMP signalling protects bacteria against viral infection. *Nature* **574**, 691–695 (2019).
3. Doron, S. et al. Systematic discovery of antiphage defense systems in the microbial pangenome. *Science* **359**, eaar4120-18 (2018).
4. Gao, L. et al. Diverse enzymatic activities mediate antiviral immunity in prokaryotes. *Science* **369**, 1077–1084 (2020).
5. Harms, A., Brodersen, D. E., Mitarai, N. & Gerdes, K. Toxins, targets, and triggers: an overview of toxin-antitoxin biology. *Mol. Cell* **70**, 768–784 (2018).
6. Song, S. & Wood, T. K. A primary physiological role of toxin/antitoxin systems is phage inhibition. *Front. Microbiol.* **11**, 1895 (2020).
7. Page, R. & Peti, W. Toxin-antitoxin systems in bacterial growth arrest and persistence. *Nat. Chem. Biol.* **12**, 208–214 (2016).
8. Ronneau, S. & Helaine, S. Clarifying the link between toxin-antitoxin modules and bacterial persistence. *J. Mol. Biol.* **431**, 3462–3471 (2019).
9. Yamaguchi, Y. & Inouye, M. Regulation of growth and death in *Escherichia coli* by toxin–antitoxin systems. *Nat. Rev. Microbiol.* **9**, 779–790 (2011).
10. LeRoux, M., Culviner, P. H., Liu, Y. J., Littlehale, M. L. & Laub, M. T. Stress can induce transcription of toxin-antitoxin systems without activating toxin. *Mol. Cell* **79**, 280–292.e8 (2020).
11. Christensen, S. K., Pedersen, K., Hansen, F. G. & Gerdes, K. Toxin–antitoxin loci as stress-response-elements: ChpAK/MazF and ChpBK cleave translated RNAs and are counteracted by tmRNA. *J. Mol. Biol.* **332**, 809–819 (2003).
12. Fineran, P. C. et al. The phage abortive infection system, ToxIN, functions as a protein-RNA toxin-antitoxin pair. *Proc. Natl Acad. Sci. USA* **106**, 894–899 (2009).
13. Guegler, C. K. & Laub, M. T. Shutoff of host transcription triggers a toxin-antitoxin system to cleave phage RNA and abort infection. *Mol. Cell* **81**, 2361–2373 (2021).
14. Koga, M., Otsuka, Y., Lemire, S. & Yonesaki, T. *Escherichia coli* rnlA and rnlB compose a novel toxin-antitoxin system. *Genetics* **187**, 123–130 (2011).
15. Makarova, K. S., Wolf, Y. I., Snir, S. & Koonin, E. V. Defense islands in bacterial and archaeal genomes and prediction of novel defense systems. *J. Bacteriol.* **193**, 6039–6056 (2011).
16. Makarova, K. S., Wolf, Y. I. & Koonin, E. V. Comparative genomics of defense systems in archaea and bacteria. *Nucleic Acids Res.* **41**, 4360–4377 (2013).
17. Jankevicius, G., Ariza, A., Ahel, M. & Ahel, I. The toxin-antitoxin system DarTG catalyzes reversible ADP-ribosylation of DNA. *Mol. Cell* **64**, 1109–1116 (2016).
18. Lawarée, E. et al. DNA ADP-ribosylation stalls replication and is reversed by recf-mediated homologous recombination and nucleotide excision repair. *Cell Rep.* **30**, 1373–1384.e4 (2020).
19. Schuller, M. et al. Molecular basis for DarT ADP-ribosylation of a DNA base. *Nature* **596**, 597–602 (2021).
20. Zaveri, A. et al. Depletion of the DarG antitoxin in *Mycobacterium tuberculosis* triggers the DNA-damage response and leads to cell death. *Mol. Microbiol.* **114**, 641–652 (2020).
21. De Souza, R. F. & Aravind, L. Identification of novel components of NAD-utilizing metabolic pathways and prediction of their biochemical functions. *Mol. Biosyst.* **8**, 1661–1677 (2012).
22. Rack, J. G. M., Perina, D. & Ahel, I. Macrodomains: structure, function, evolution, and catalytic activities. *Annu. Rev. Biochem.* **85**, 431–454 (2016).
23. Tromans-Coia, C. et al. TARG1 protects against toxic DNA ADP-ribosylation. *Nucleic Acids Res.* https://doi.org/10.1093/nar/gkab771 (2021).
24. Otsuka, Y. & Yonesaki, T. Dmd of bacteriophage T4 functions as an antitoxin against *Escherichia coli* LsoA and RnlA toxins. *Mol. Microbiol.* **83**, 669–681 (2012).
25. McCorquodale, D. J. & Warner, H. R. in *The Bacteriophages* (ed. Calendar, R.) 439–475 (Springer, 1988); https://doi.org/10.1007/978-1-4684-5424-6_10
26. Ando, Y. et al. ELTA: enzymatic labeling of terminal ADP-ribose. *Mol. Cell* **73**, 845–856.e5 (2019).
27. Srikant, S., Guegler, C. K. & Laub, M. T. The evolution of a counter-defense mechanism in a virus constrains its host range. Preprint at *bioRxiv* https://doi.org/10.1101/2022.04.14.488369 (2022).
28. Petrov, V. M., Ratnayaka, S., Nolan, J. M., Miller, E. S. & Karam, J. D. Genomes of the T4-related bacteriophages as windows on microbial genome evolution. *Virol. J.* **7**, 292 (2010).
29. Warner, H. R., Drong, R. F. & Berget, S. M. Early events after infection of *Escherichia coli* by bacteriophage T5. Induction of a 5'-nucleotidase activity and excretion of free bases. *J. Virol.* **15**, 273–280 (1975).
30. Pinilla-Redondo, R. et al. Discovery of multiple anti-CRISPRs highlights anti-defense gene clustering in mobile genetic elements. *Nat. Commun.* **11**, 5652 (2020).
31. Bondy-Denomy, J. et al. Prophages mediate defense against phage infection through diverse mechanisms. *ISME J.* **10**, 2854–2866 (2019).
32. Dedrick, R. M. et al. Prophage-mediated defence against viral attack and viral counter-defence. *Nat. Microbiol.* **2**, 16251 (2017).
33. Rousset, F., Dowding, J., Bernheim, A., Rocha, E. P. C. & Bikard, D. Prophage-encoded hotspots of bacterial immune systems. Preprint at *bioRxiv* https://doi.org/10.1101/2021.01.21.427644 (2021).
34. Hallez, R. et al. New toxins homologous to ParE belonging to three-component toxin–antitoxin systems in *Escherichia coli* O157:H7. *Mol. Microbiol.* **76**, 719–732 (2010).
35. Peltier, J. et al. Type I toxin-antitoxin systems contribute to the maintenance of mobile genetic elements in *Clostridioides difficile*. *Commun. Biol.* **3**, 718 (2020).
36. Yao, J. et al. Type II toxin/antitoxin system ParESO /CopASO stabilizes prophage CP4So in *Shewanella oneidensis*. *Environ. Microbiol.* **20**, 1224–1239 (2018).
37. Chen, I.-M. A. et al. IMG/M v.5.0: an integrated data management and comparative analysis system for microbial genomes and microbiomes. *Nucleic Acids Res.* **47**, D666–D677 (2019).
38. Steinegger, M. & Söding, J. MMseqs2 enables sensitive protein sequence searching for the analysis of massive data sets. *Nat. Biotechnol.* **35**, 1026–1028 (2017).
39. Bobonis, J. et al. Bacterial retrons encode tripartite toxin/antitoxin systems. Preprint at *bioRxiv* https://doi.org/10.1101/2020.06.22.160168 (2020).
40. Chung, C. T., Niemela, S. L. & Miller, R. H. One-step preparation of competent *Escherichia coli*: transformation and storage of bacterial cells in the same solution. *Proc. Natl Acad. Sci. USA* **86**, 2172–2175 (1989).
41. Haldimann, A. & Wanner, B. L. Conditional-replication, integration, excision, and retrieval plasmid-host systems for gene structure-function studies of bacteria. *J. Bacteriol.* **183**, 6384–6393 (2001).
42. Blomfield, I. C., Vaughn, V., Rest, R. F. & Eisenstein, B. I. Allelic exchange in *Escherichia coli* using the *Bacillus subtilis* sacB gene and a temperature-sensitive pSC101 replicon. *Mol. Microbiol.* **5**, 1447–1457 (1991).

43. Datsenko, K. A. & Wanner, B. L. One-step inactivation of chromosomal genes in *Escherichia coli* K-12 using PCR products. *Proc. Natl Acad. Sci. USA* **97**, 6640–6645 (2000).
44. Duong, M. M., Carmody, C. M., Ma, Q., Peters, J. E. & Nugen, S. R. Optimization of T4 phage engineering via CRISPR/Cas9. *Sci. Rep.* **10**, 18229 (2020).
45. Jiang, W., Bikard, D., Cox, D., Zhang, F. & Marraffini, L. A. RNA-guided editing of bacterial genomes using CRISPR-Cas systems. *Nat. Biotechnol.* **31**, 233–239 (2013).

Acknowledgements

M.L. was supported by a postdoctoral fellowship from the Charles A. King Trust Postdoctoral Research Fellowship Program, Bank of America, N.A., Co-Trustees. This work was funded by an NIH grant to M.T.L. (R01GM082899), who is also an Investigator of the Howard Hughes Medical Institute; the Sagol Weizmann-MIT Bridge Program (M.T.L. and R.S.); and grants to R.S.: the European Research Council (grant ERC-CoG 681203), the Ernest and Bonnie Beutler Research Program of Excellence in Genomic Medicine, and the German Research Council (DFG) priority program SPP 2330 (grant SO 1611/2). A.K.L.L. was supported by an NIH grant (R01GM104135).

Author contributions

M.L. performed all experiments. S.S. helped with the construction of phage gene deletions and plaque assays, and with design and interpretation of phage evolution experiments. G.I.C.T. helped with strain construction, bacterial and phage growth and survival assays, and DNA extraction and sequencing. T.Z. helped with the cysteine and methionine incorporation assays. M.L.L. helped with bacterial and phage growth and survival experiments. M.B. and A.K.L.L. supplied biochemical reagents and controls and helped with design of ELTA assays. S.D. and R.S. performed a bioinformatic analysis of TA proximity to known defence elements. M.L. and M.T.L. designed experiments, analysed data, prepared figures and wrote the manuscript.

Competing interests

R.S. is a scientific cofounder and advisor of BiomX and Ecophage.

Additional information

Extended data is available for this paper at https://doi.org/10.1038/s41564-022-01153-5.

Supplementary information The online version contains supplementary material available at https://doi.org/10.1038/s41564-022-01153-5.

Correspondence and requests for materials should be addressed to Michael T. Laub.

Peer review information *Nature Microbiology* thanks the anonymous reviewers for their contribution to the peer review of this work.

Reprints and permissions information is available at www.nature.com/reprints.

Publisher's note Springer Nature remains neutral with regard to jurisdictional claims in published maps and institutional affiliations.

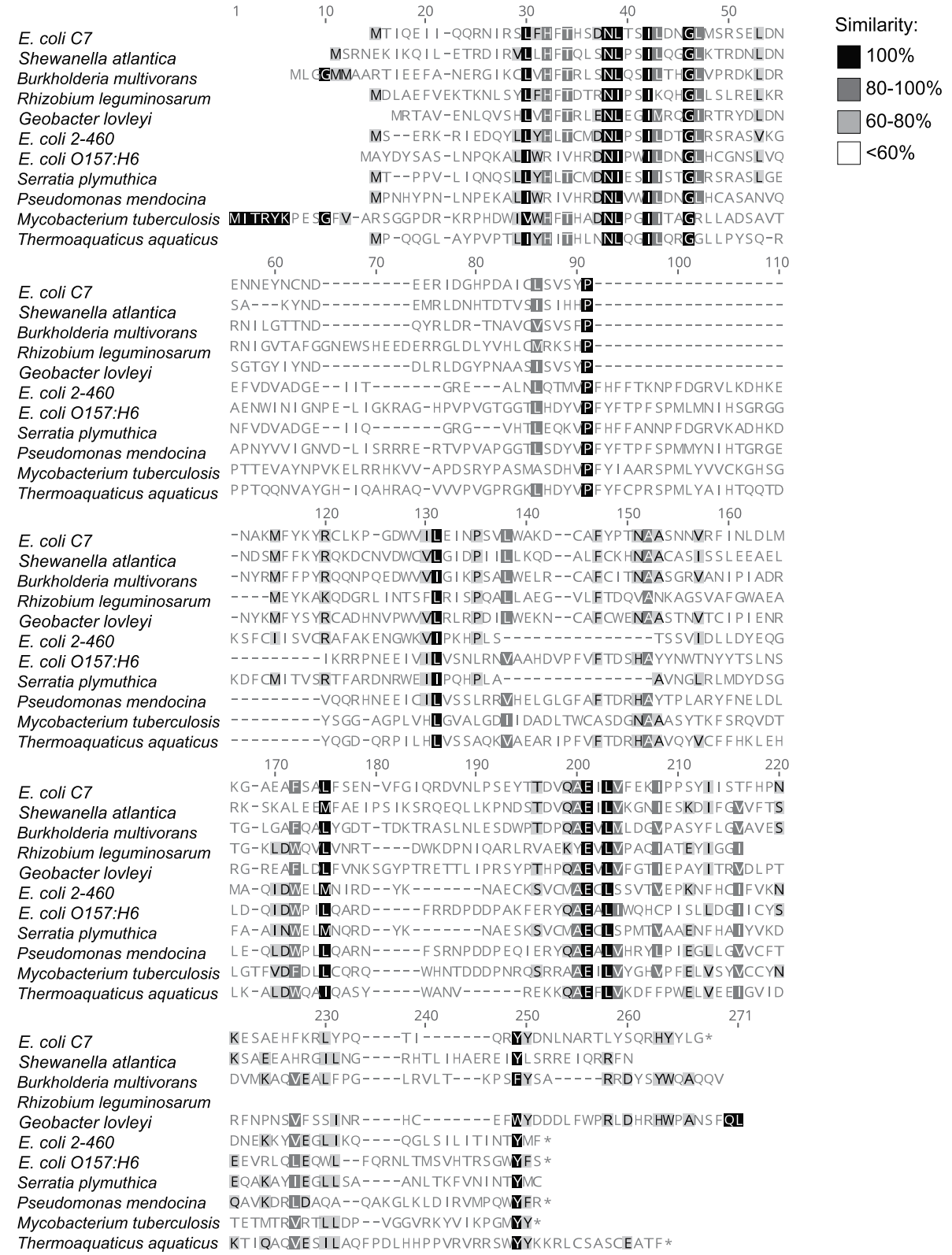

Extended Data Fig. 1 | Sequence alignment of DarT homologs. Full multiple sequence alignments of representative DarT homologs corresponding to Fig. 1f.

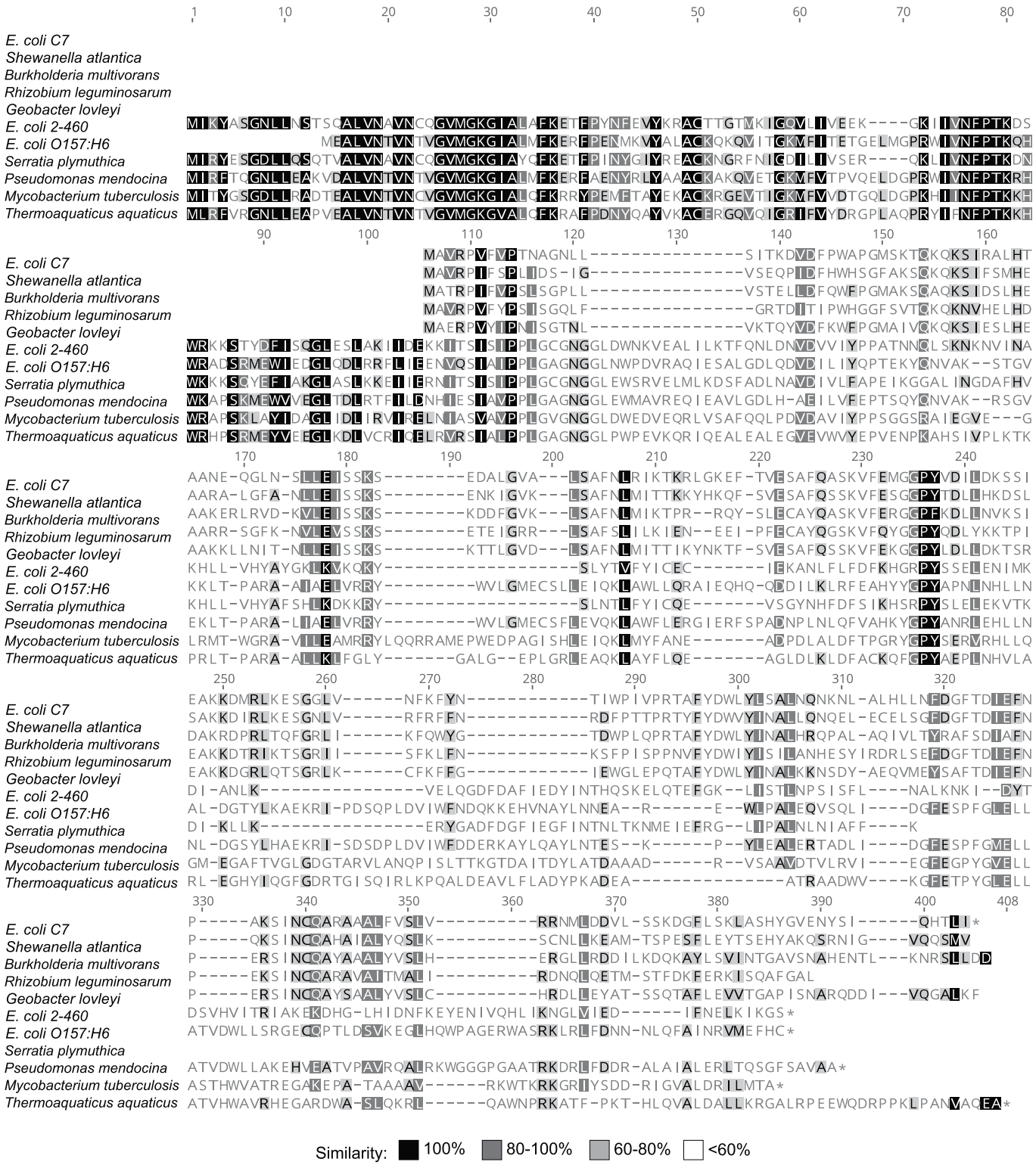

Extended Data Fig. 2 | Sequence alignment of DarG homologs. Full multiple sequence alignments of representative DarG homologs corresponding to Fig. 1f.

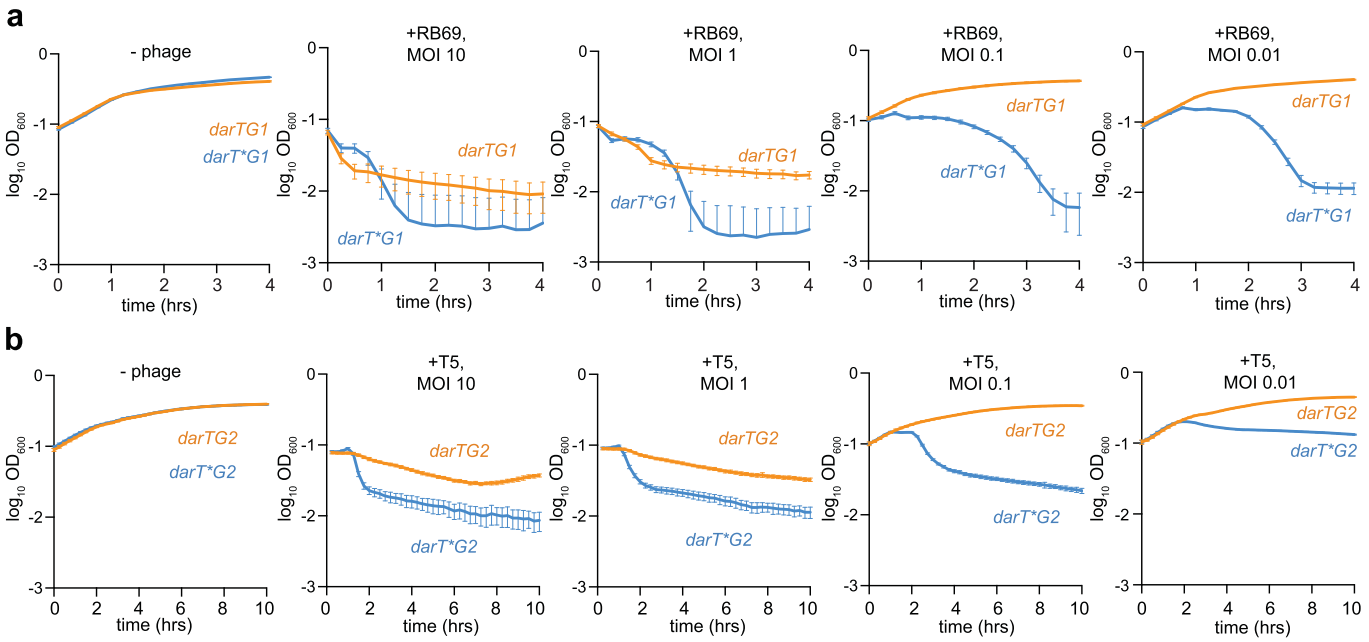

Extended Data Fig. 3 | DarTG systems provide phage defense via an abortive infection mechanism. Growth curves for strains with the indicated plasmid-encoded TA system after infection with RB69 (a) or T5 (b) phage at varying multiplicities of infection (MOI). The mean and S.D. of 6-12 technical replicates are presented; data are an independent biological replicate for data presented in Fig. 2a, b.

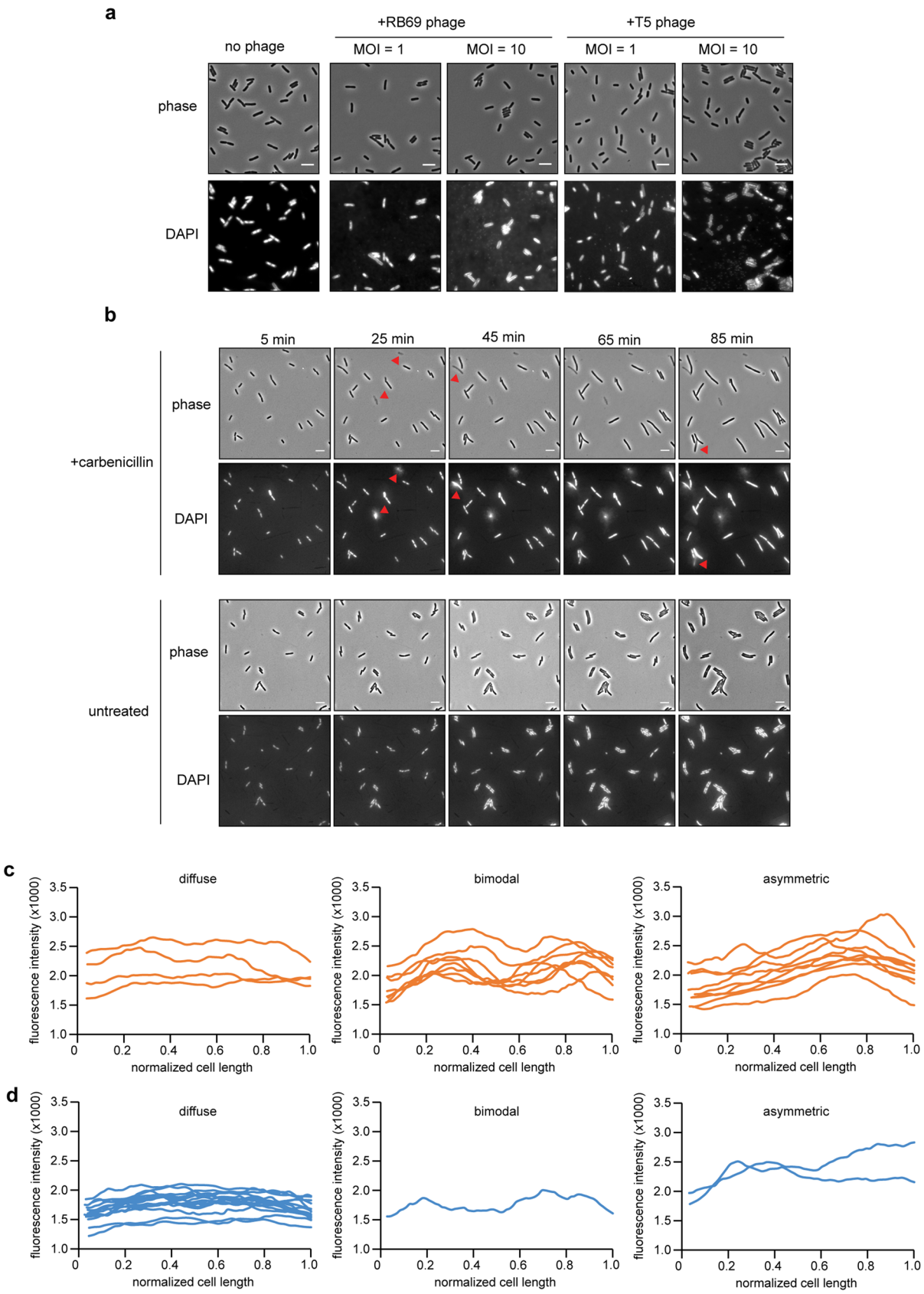

Extended Data Fig. 4 | DAPI-staining detects phage particles and changes in DNA compaction in infected cells. a, Snapshots taken of cultures of *E. coli* MG1655 cells containing DAPI 10-20 min after addition of the indicated phage. **b**, Time-lapse series of DAPI-stained *E. coli* MG1655 cells on agarose pads containing 100 μg/mL carbenicillin (top) or untreated (bottom). Lysed cells are indicated with red arrows. **c**–**d**, Fluorescence intensity profiles of individual cells are plotted for DarTG1 (c) or DarT*G1 (d) cells. Profiles for 18-20 representative cells are shown for each condition and are grouped into diffuse (left), bimodal (middle), or asymmetric (right). Scale bars, 4 μM.

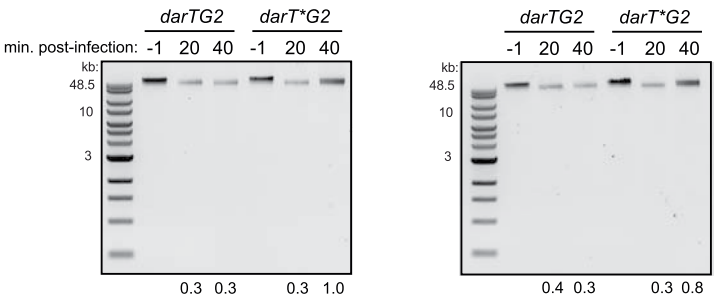

Extended Data Fig. 5 | Less DNA is recovered from infected cells when a DarTG2 system is present. Total DNA extracted from cells containing darTG2 or darT*G2 and infected with T5 for the times indicated. The intensity of the band at each time post-infection relative to the pre-infection band is reported at the bottom. Two independent replicates are shown.

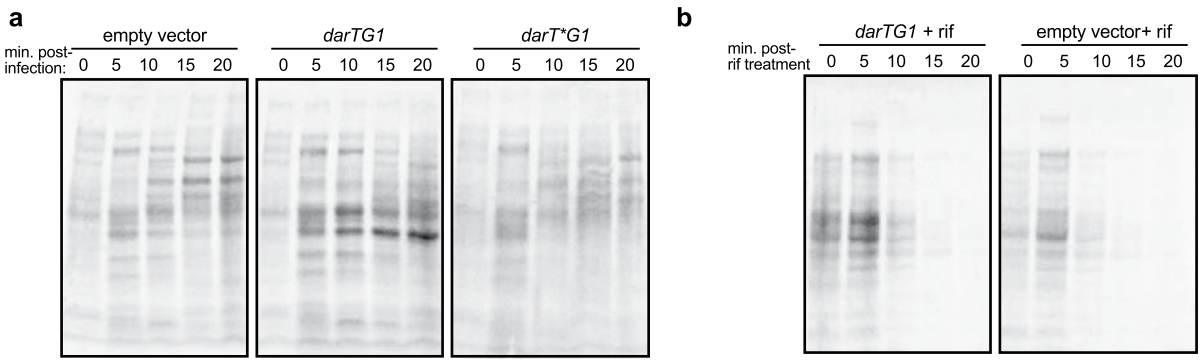

Extended Data Fig. 6 | Activated DarT inhibits the timing of phage protein production. Protein synthesis rates as measured by ^{35}S-labeled cysteine and methionine incorporation at various time points after infection for *E. coli* bearing the indicated plasmids and infected with either RB69 at MOI 5 (**a**) or treated with 300 μg/mL rifampicin (rif) (**b**). Data shown are representative of 2 independent biological replicates.

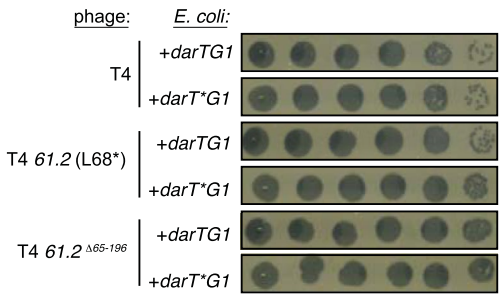

Extended Data Fig. 7 | Gene *61.2* is not essential in T4. Plaque assays of the wild-type T4, or variants with either a premature stop-codon in gp61.2 (L68*) or a large deletion of residues 65-196 (T4 61.2$^{\Delta 65\text{-}196}$) on *E. coli* with an active or inactive version of the DarTG1 system.

nature portfolio

Corresponding author(s): Laub

Last updated by author(s): May 11, 2022

Reporting Summary

Nature Portfolio wishes to improve the reproducibility of the work that we publish. This form provides structure for consistency and transparency in reporting. For further information on Nature Portfolio policies, see our Editorial Policies and the Editorial Policy Checklist.

Statistics

For all statistical analyses, confirm that the following items are present in the figure legend, table legend, main text, or Methods section.

n/a	Confirmed	
☐	☒	The exact sample size (*n*) for each experimental group/condition, given as a discrete number and unit of measurement
☐	☒	A statement on whether measurements were taken from distinct samples or whether the same sample was measured repeatedly
☐	☒	The statistical test(s) used AND whether they are one- or two-sided *Only common tests should be described solely by name; describe more complex techniques in the Methods section.*
☒	☐	A description of all covariates tested
☒	☐	A description of any assumptions or corrections, such as tests of normality and adjustment for multiple comparisons
☐	☒	A full description of the statistical parameters including central tendency (e.g. means) or other basic estimates (e.g. regression coefficient) AND variation (e.g. standard deviation) or associated estimates of uncertainty (e.g. confidence intervals)
☐	☒	For null hypothesis testing, the test statistic (e.g. *F*, *t*, *r*) with confidence intervals, effect sizes, degrees of freedom and *P* value noted *Give P values as exact values whenever suitable.*
☒	☐	For Bayesian analysis, information on the choice of priors and Markov chain Monte Carlo settings
☒	☐	For hierarchical and complex designs, identification of the appropriate level for tests and full reporting of outcomes
☒	☐	Estimates of effect sizes (e.g. Cohen's *d*, Pearson's *r*), indicating how they were calculated

Our web collection on statistics for biologists contains articles on many of the points above.

Software and code

Policy information about availability of computer code

Data collection	MetaMorph v7.10.2.240 (Molecular Devices LLC) was used to collect microscopy data. Biotek Gen5 v. 3.02 was used to collect growth curve data.
Data analysis	Geneious Prime v2020.0.5 and v20212.2 (Biomatters) were used to process and analyze all DNA sequencing data. Prism 9 for macOS (Version 9.2.0) was used to produce graphs and execute statistical analyses. Fiji v 1.0 was used for analyzing microscopy images. Microsoft Excel for Mac (v 16.60) was used for smoothing sequencing data (Fig. 3e, g) and microscopy line scans (Extended Data 4c). Matlab r2017a was used to analyze plate reader data.

For manuscripts utilizing custom algorithms or software that are central to the research but not yet described in published literature, software must be made available to editors and reviewers. We strongly encourage code deposition in a community repository (e.g. GitHub). See the Nature Portfolio guidelines for submitting code & software for further information.

Data

Policy information about availability of data

All manuscripts must include a data availability statement. This statement should provide the following information, where applicable:

- Accession codes, unique identifiers, or web links for publicly available datasets
- A description of any restrictions on data availability
- For clinical datasets or third party data, please ensure that the statement adheres to our policy

The bioinformatic analysis was performed using protein sequences available in the Integrated Microbial Genomes (IMG) database (https://img.jgi.doe.gov/). DarTG1 and DarTG2 were identified in Escherichia coli C7 (NCBI Accession GCA_001901425.1) and Escherichia coli 2-460-02_S4_C3 (NCBI Accession GCA_000704545.1).

Sequencing data are available on NCBI (BioProject PRJNA776027). Sequencing data were aligned to reference genomes of MG1655 (Accession number CP025268.1), RB69 (Accession number NC_004928), SECΦ18 (accession number LT960609), or T5 (accession number NC_005859.1). All other source data has been deposited to Mendeley Data, V1, doi: 10.17632/v9bmr549nf.1.

Field-specific reporting

Please select the one below that is the best fit for your research. If you are not sure, read the appropriate sections before making your selection.

☒ Life sciences ☐ Behavioural & social sciences ☐ Ecological, evolutionary & environmental sciences

For a reference copy of the document with all sections, see nature.com/documents/nr-reporting-summary-flat.pdf

Life sciences study design

All studies must disclose on these points even when the disclosure is negative.

Sample size	Sample sizes were chosen based on the number needed to reliably determine differences between groups. All experiments were performed at 2-3 times independently.
Data exclusions	No data were excluded.
Replication	All experiments were independently replicated at least twice.
Randomization	This study does not involve subjects that require randomization.
Blinding	This study does not involve procedures that require blinding.

Reporting for specific materials, systems and methods

We require information from authors about some types of materials, experimental systems and methods used in many studies. Here, indicate whether each material, system or method listed is relevant to your study. If you are not sure if a list item applies to your research, read the appropriate section before selecting a response.

Materials & experimental systems

n/a	Involved in the study
☐	☒ Antibodies
☒	☐ Eukaryotic cell lines
☒	☐ Palaeontology and archaeology
☒	☐ Animals and other organisms
☒	☐ Human research participants
☒	☐ Clinical data
☒	☐ Dual use research of concern

Methods

n/a	Involved in the study
☒	☐ ChIP-seq
☒	☐ Flow cytometry
☒	☐ MRI-based neuroimaging

Antibodies

Antibodies used	Poly/Mono-ADP Ribose (Clone E6F6A); Cell Signaling, Catalog #83732; Lot # 3.
Validation	Manufacturer specifies that species reactivity is determined by testing in at least one approved application (e.g., western blot). Antibody was validated for detection of DNA ADP-ribosylation in Schuller et. al. (2021) Nature. We performed internal validation using an in vitro generated control DNA oligo that had been ADP-ribosylated, compared to the un-ribosylated oligo.